

SIMBIG: Mock Challenge for a Forward Modeling Approach to Galaxy Clustering

CHANGHOON HAHN,^{1,*} MICHAEL EICKENBERG,² SHIRLEY HO,³ JIAMIN HOU,^{4,5} PABLO LEMOS,^{6,7,2}
 ELENA MASSARA,^{8,9} CHIRAG MODI,^{2,3} AZADEH MORADINEZHAD DIZGAH,¹⁰
 BRUNO RÉGALDO-SAINT BLANCARD,² AND MUNTAZIR M. ABIDI¹⁰

¹*Department of Astrophysical Sciences, Princeton University, Princeton NJ 08544, USA*

²*Center for Computational Mathematics, Flatiron Institute, 162 5th Avenue, New York, NY 10010, USA*

³*Center for Computational Astrophysics, Flatiron Institute, 162 5th Avenue, New York, NY 10010, USA*

⁴*Department of Astronomy, University of Florida, 211 Bryant Space Science Center, Gainesville, FL 32611, USA*

⁵*Max-Planck-Institut für Extraterrestrische Physik, Postfach 1312, Giessenbachstrasse 1, 85748 Garching bei München, Germany*

⁶*Department of Physics, Université de Montréal, Montréal, 1375 Avenue Thérèse-Lavoie-Roux, QC H2V 0B3, Canada*

⁷*Mila - Quebec Artificial Intelligence Institute, Montréal, 6666 Rue Saint-Urbain, QC H2S 3H1, Canada*

⁸*Waterloo Centre for Astrophysics, University of Waterloo, 200 University Ave W, Waterloo, ON N2L 3G1, Canada*

⁹*Department of Physics and Astronomy, University of Waterloo, 200 University Ave W, Waterloo, ON N2L 3G1, Canada*

¹⁰*Département de Physique Théorique, Université de Genève, 24 quai Ernest Ansermet, 1211 Genève 4, Switzerland*

ABSTRACT

Simulation-Based Inference of Galaxies (SIMBIG) is a forward modeling framework for analyzing galaxy clustering using simulation-based inference. In this work, we present the SIMBIG forward model, which is designed to match the observed SDSS-III BOSS CMASS galaxy sample. The forward model is based on high-resolution QUIJOTE N -body simulations and a flexible halo occupation model. It includes full survey realism and models observational systematics such as angular masking and fiber collisions. We present the “mock challenge” for validating the accuracy of posteriors inferred from SIMBIG using a suite of 1,500 test simulations constructed using forward models with a different N -body simulation, halo finder, and halo occupation prescription. As a demonstration of SIMBIG, we analyze the power spectrum multipoles out to $k_{\text{max}} = 0.5 h/\text{Mpc}$ and infer the posterior of ΛCDM cosmological and halo occupation parameters. Based on the mock challenge, we find that our constraints on Ω_m and σ_8 are unbiased, but conservative. Hence, the mock challenge demonstrates that SIMBIG provides a robust framework for inferring cosmological parameters from galaxy clustering on non-linear scales and a complete framework for handling observational systematics. In subsequent work, we will use SIMBIG to analyze summary statistics beyond the power spectrum including the bispectrum, marked power spectrum, skew spectrum, wavelet statistics, and field-level statistics.

Keywords: cosmological parameters from LSS — Machine learning — cosmological simulations — galaxy surveys

1. INTRODUCTION

The spatial distribution of galaxies contains key cosmological information about our Universe. From the statistical clustering of galaxies, we can measure the expansion history of the Universe and the growth of structure (Sargent & Turner 1977; Kaiser 1987; Eisenstein et al. 1998; Hamilton 1998; Seo & Eisenstein 2003). With these measurements we can probe the nature of dark energy and test theories of gravity (*e.g.* Jain et al. 2013; Kim et al. 2015; Huterer et al. 2015). Precise measurements of galaxy clustering can also be used to test inflation (Liddle & Lyth 2000; Dalal et al. 2008; Slosar et al. 2008; Ho et al. 2015) and measure the sum of neutrino masses (Font-Ribera et al. 2014; Beutler et al. 2014, see Lesgourgues et al. 2013 for a review).

Upcoming galaxy surveys will collect an unprecedented amount of data to take advantage of this cosmological information and produce the most precise measurements of galaxy clustering. In particular, spectroscopic galaxy surveys will be conducted using the Dark Energy Spectroscopic Instrument (DESI; Collaboration et al. 2016a,b; Abareshi et al. 2022), the Subaru Prime Focus Spectrograph (PFS; Takada et al. 2014; Tamura et al. 2016), the ESA *Euclid* satellite mission (Laureijs et al. 2011), and the Nancy Grace Roman Space Telescope (Roman; Spergel et al. 2015; Wang et al. 2022a) over the next decade. They will precisely measure the three-dimensional clustering of galaxies over unprecedented cosmic volumes. Combined with constraints from other cosmological probes, such as the cosmic microwave background (CMB), these surveys will produce the most precise constraints on the cosmological parameters. Moreover, they will precisely test the standard Λ CDM model and enable us to search for new physics beyond the standard paradigm.

The current standard analyses for galaxy clustering use theoretical models of galaxy clustering from perturbation theory of large-scale structure (PT; Beutler et al. 2017; Ivanov et al. 2020, see Bernardeau et al. 2002 and Desjacques et al. 2016 for a review). These standard analyses have major limitations. First, PT models cannot accurately model non-linear galaxy clustering. The primary analyses of the Sloan Digital Sky Survey (SDSS)-III Baryon Oscillation Spectroscopic Survey (BOSS; Eisenstein et al. 2011; Dawson et al. 2013) only model the galaxy power spectrum, the two-point clustering statistic, to $k_{\text{max}} < 0.2 h/\text{Mpc}$ (*e.g.* Beutler et al. 2014, 2017; Grieb et al. 2017). Even recent models that use an effective field theory approach with non-linear biasing, IR resummation, and “counterterms” (*e.g.* Carrasco et al. 2012; Senatore & Zaldarriaga 2014; Senatore 2015; Perko et al. 2016; Ivanov et al. 2020; D’Amico et al. 2022) are limited to $k_{\text{max}} \sim 0.2 h/\text{Mpc}$. For the bispectrum, the lowest higher-order three-point statistic, analyses can only include measurements out to $k \leq 0.08 h/\text{Mpc}$ (Philcox & Ivanov 2021). D’Amico et al. (2022) extend their analysis to $k \sim 0.2 h/\text{Mpc}$ for the bispectrum monopole but they required 33 additional parameters.

Another limitation is that standard galaxy clustering analyses assume that the likelihood used in their Bayesian parameter inference has a Gaussian form. This assumption relies on the central limit theorem, which breaks down on large scales with low signal-to-noise and on small scales where modes are highly correlated. Hahn et al. (2019) found that the non-Gaussianity of the likelihood can significantly bias the overall parameter constraints. The effect may be more pronounced at the

* changhoon.hahn@princeton.edu.com

precision level of upcoming surveys and for observables beyond the power spectrum. Lastly, standard galaxy clustering analyses rely on corrections to the clustering measurements, typically through weights imposed on galaxies, to account for observational systematics. While some systematics can be successfully corrected with weights, others like fiber collision pose serious challenges for upcoming surveys. Improved correction schemes for fiber collisions may be sufficient for power spectrum analyses (Guo et al. 2012; Hahn et al. 2017a; Pinol et al. 2017; Bianchi et al. 2018; Smith et al. 2019). Nevertheless, no correction schemes have yet been designed or demonstrated for higher-order statistics.

Meanwhile, there is a growing consensus among forecasts that there is significant cosmological information in higher-order statistics and on non-linear scales. For example, Hahn & Villaescusa-Navarro (2021) recently used the QUIJOTE suite of simulations to forecast the cosmological information content of the redshift-space galaxy bispectrum. They found that constraints on cosmological parameters Ω_m , Ω_b , h , n_s , and σ_8 improve by more than a factor of 2 when the bispectrum is included. Including smaller scales ($0.2 < k < 0.5 h/\text{Mpc}$) also tightens constraints by an additional factor of 2. Similar forecasts made using other higher-order statistics, *e.g.* the marked power spectrum (Massara et al. 2020, 2022), the reconstructed power spectrum (Wang et al. 2022b), the skew spectra (Hou et al. 2022), wavelet statistics (Eickenberg et al. 2022), find consistent improvements over the power spectrum. Despite the advantages that these observables promise, the limitations above prevent most of them from being analyzed within the standard galaxy clustering analysis framework.

In this work, we present the Simulation-Based Inference of Galaxies (SIMBIG), an alternative approach to analyzing galaxy clustering that addresses each of the major limitations of standard galaxy clustering analyses. First, SIMBIG uses simulated forward models of the galaxy distribution. As a result, it can accurately model galaxy clustering on non-linear scales beyond the limits of PT. Furthermore, we can analyze any observable (*i.e.* summary statistic) that can be measured in the observed galaxy distribution. Second, SIMBIG uses simulation-based inference (SBI; also known as “likelihood-free inference” or “implicit likelihood inference”) that enables rigorous inference using only a forward model of the observables. It makes no assumptions on the functional form of the likelihood. It leverages the machine learning based density estimation to accurately describe even high-dimensional posteriors efficiently with a limited number of simulations (see Cranmer et al. 2020 and references therein). SBI has already been used for Bayesian inference in large-scale structure studies (*e.g.* Hahn et al. 2017b; Alsing et al. 2019; Hassan et al. 2021; Jeffrey et al. 2021; Makinen et al. 2021; Lemos et al. 2022). It has also been widely adopted in broader astronomical contexts (Dax et al. 2021; Huppenkothen & Bachetti 2021; Lemos et al. 2021; Tortorelli et al. 2021; Zhang et al. 2021; Hahn & Melchior 2022; Lemos et al. 2022). Lastly, SIMBIG provides a more complete framework for accounting for observational systematics. Unlike the conventional approach of using weights to correct for systematics, the forward model in SIMBIG includes the systematics. Some observational systematics are often much easier to model than to correct in the clustering measurements and by forward modeling them a correction scheme does not need to be developed for every summary statistic. Altogether, SIMBIG provides a framework that can robustly analyze galaxy clustering down to non-linear scales and with higher-order statistics.

In this work and in an accompanying paper (Hahn et al. 2022, hereafter H22a), we demonstrate SIMBIG by applying it to BOSS. As the first papers of a series, we apply SIMBIG to the power spectrum multipoles, $P_\ell(k)$, so that we can validate the SIMBIG framework in detail and make comparisons to previous galaxy clustering studies in the literature. H22a presents the cosmological constraints and briefly describes SIMBIG. In this work, we describe the details of SIMBIG pipeline: the forward model and the SBI framework. We also present the mock challenge for validating the accuracy of the SIMBIG posteriors using a suite of test simulations constructed with different forward models. In subsequent works, we will apply SIMBIG to summary statistics beyond the power spectrum including the bispectrum, the marked power spectrum, the skew spectra, the void probability function, and wavelet statistics. We will also analyze field-level summary statistics that compress all the information in the galaxy field using convolutional and graph neural networks.

We begin in Section 2 by describing the observational galaxy sample that we analyze with SIMBIG. Then, we present the details of the SIMBIG pipeline in Section 3. Afterwards, in Section 4, we describe how we construct the suite of test simulations used for the mock challenge. We present the results of the mock challenge in Section 5 and discuss our findings in Section 6.

2. OBSERVATIONS: BOSS CMASS GALAXIES

We apply SIMBIG to the publicly available galaxy catalog¹ from the Sloan Digital Sky Survey (SDSS)-III Baryon Oscillation Spectroscopic Survey (BOSS) Data Release 12 (Eisenstein et al. 2011; Dawson et al. 2013). BOSS observed two galaxy samples, LOWZ and CMASS, that span the redshift ranges $0.2 \lesssim z \lesssim 0.5$ and $0.43 < z < 0.7$. In this work, we focus on the CMASS galaxy sample, which consists of Luminous Red Galaxies (LRGs) with a prominent 4000Å break in their spectral energy distribution for reliable redshift measurements. CMASS LRGs reside in massive halos with $M_h \gtrsim 10^{13} M_\odot$ and the sample has a comoving galaxy number density of $\bar{n} \approx 3 \times 10^{-4} h^3 \text{Mpc}^{-3}$ (White et al. 2011; Leauthaud et al. 2016; Saito et al. 2016; Reid et al. 2016; Zhai et al. 2017).

Each CMASS galaxy is assigned a set of weights to account for incompleteness and observational systematics in BOSS. These systematics include redshift failures, fiber collisions, and variations in the target density caused by stellar density and seeing conditions. We refer readers to Ross et al. (2012, 2017) for more details on the observational systematics in BOSS.

In this work, we further restrict our analysis to CMASS galaxies in the Southern Galactic Cap (SGC) that have $\text{Dec} > -6^\circ$ and $-25^\circ < \text{RA} < 28^\circ$. We also impose a redshift cut of $0.45 < z < 0.6$. As we discuss later in Section 3.3, we impose these extra restrictions on the CMASS sample due to the limited volume of the simulations used in our forward model. In the top panels of Figure 1, we present the spatial and angular distributions of the CMASS-SGC sample (blue). The left and center panels present the 3D distribution of CMASS-SGC galaxies at two different viewing angles. The right panel presents the angular distribution. Figure 1 illustrates the extra selections that we impose and the overall distribution of the 109,636 CMASS-SGC galaxies.

¹ <https://data.sdss.org/sas/dr12/booss/lss/>

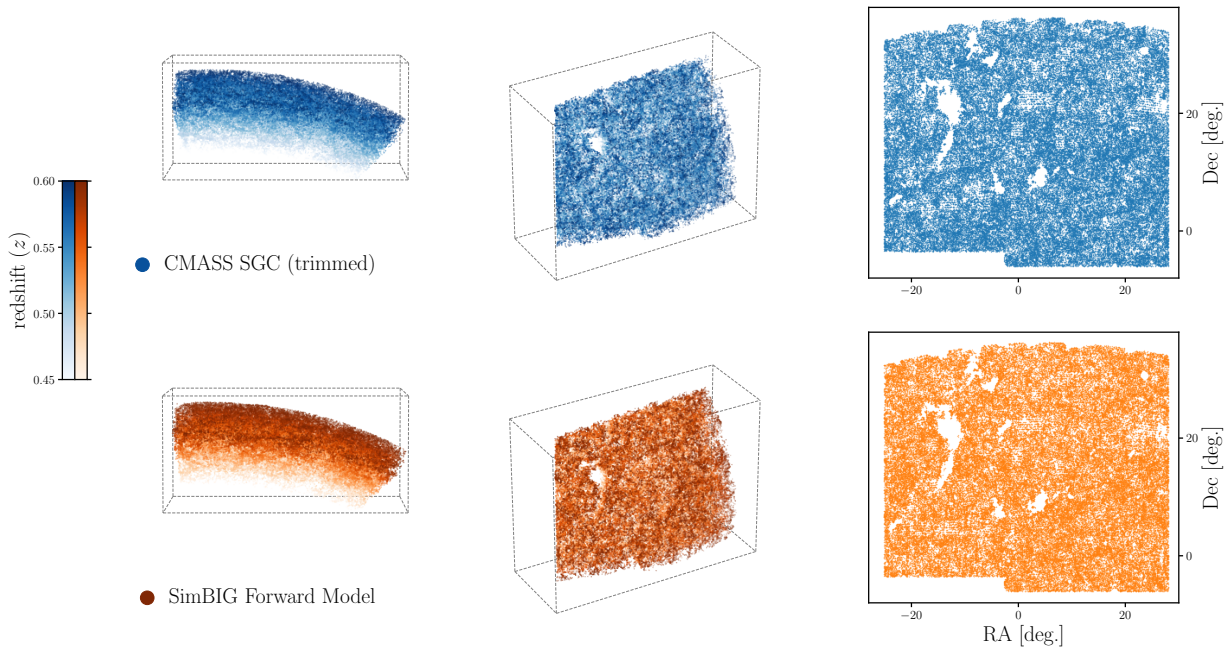


Figure 1. Comparison of the observed CMASS-SGC galaxy sample (top; blue) with the SIMBIG forward model (bottom; orange). We present the 3D distribution of galaxies at two different viewing angles in the left and center panels. The right panels plot the angular distribution of galaxies. Our CMASS-SGC galaxy sample contains 109,636 galaxies. Our forward model constructs realistic CMASS-like galaxy samples from QUIJOTE N -body simulations using an HOD model that includes the effects of assembly bias, concentration bias, and velocity biases for central and satellite galaxies. It also applies observational systematics: the CMASS survey geometry, veto masks, and fiber collisions. Hence, our forward modeled galaxy catalogs have a selection function that closely matches the selection function of CMASS. For more comparisons of the 3D distributions, we refer readers to [Figure 1](#).

3. SIMULATION-BASED INFERENCE OF GALAXIES (SIMBIG)

3.1. Forward Model

For our forward model, we start with the N -body simulations from the QUIJOTE suite (Villaescusa-Navarro et al. 2020). In particular, we use the set of high-resolution Λ CDM Latin-hypercube (LHC) simulations. The simulations are run using the TreePM GADGET-III code. They are constructed using 1024^3 cold dark matter (CDM) particles initialized at $z = 127$ using 2LPT and gravitationally evolved until $z = 0.5$. The simulations have a cosmological volume of $1(h^{-1}\text{Gpc})^3$. By using N -body simulations, instead of more approximate schemes such as particle mesh, we can accurately model the clustering of matter down to small, non-linear scales.

In this work, our goal is to forward model the spatial distribution of galaxies. We use the halo occupation distribution (HOD; Berlind & Weinberg 2002; Zheng et al. 2007) framework to construct galaxy samples from the N -body simulations. First, we identify dark matter halos from the simula-

tions using the ROCKSTAR halo finder (Behroozi et al. 2013). ROCKSTAR identifies halos using phase space information of the dark matter particles in the simulation and has been shown to accurately determine the location of halos and resolve their substructure (Knebe et al. 2011).

Next, we populate the dark matter halos with galaxies using a state-of-the-art HOD model that includes assembly, concentration, and velocity biases. An HOD model provides the statistical prescription for determining the number of galaxies as well as their positions and velocities within the halo based on its properties. Our HOD model is based on the standard Zheng et al. (2007) model (hereafter Z07). In this model, the number of central and satellite galaxies in a halo is determined by the mass of the halo, M_h , and five free HOD parameters: $\log M_{\min}$, $\sigma_{\log M}$, $\log M_0$, $\log M_1$, α (see Table 1 for a brief description of each parameter). Central galaxies are placed at the center of the halos and with the same velocity as the halo. The positions and velocities of satellite galaxies are sampled according to a NFW (Navarro et al. 1997) profile.

While the Z07 HOD model has been shown to successfully reproduce the clustering of CMASS galaxies (White et al. 2011; Reid et al. 2014; Manera et al. 2015), a growing number of works now suggest that galaxies occupy halos in ways that depend on halo properties beyond M_h , such as the assembly history of halos (Gao et al. 2005; Wechsler et al. 2006; Zentner 2007; Dalal et al. 2008; Lacerna & Padilla 2011; Miyatake et al. 2016; More et al. 2016; Zentner et al. 2016; Vakili & Hahn 2019; Hadzhiyska et al. 2021; Hadzhiyska et al. 2022). We include this “assembly bias” effect by supplementing the Z07 model using a decorated HOD prescription (Hearin et al. 2016). For a given M_h , halos are split into two bins based on their concentrations. The high- and low-concentration halos are assigned different numbers of central and satellite galaxies but the average occupation of both populations is the same as the Z07 model. The difference is controlled by A_{bias} , a parameter that ranges from -1 to 1. For more positive values of A_{bias} , high-concentration halos host more galaxies relative to low-concentration ones of the same mass. With this prescription, our HOD depends not only on M_h but also on the halo concentration, which is a proxy for its assembly history (Mao et al. 2015).

We add extra flexibility to our HOD model by including concentration and velocity biases. Concentration bias allows the concentration of satellites galaxies to deviate from the NFW profile of their halos. We parameterize concentration bias using the free parameter η_{conc} , which sets the ratio between the concentration of satellites and halos $c_{\text{sat}}/c_{\text{halo}}$. Meanwhile, central and satellite velocity biases rescale the velocity of central and satellite galaxies with respect to the host halo. We use parameters η_{cen} , η_{sat} that set the velocity dispersions of central and satellite galaxies: $\sigma_{\text{cen}} = \eta_{\text{cen}}\sigma_{\text{halo}}$ and $\sigma_{\text{sat}} = \eta_{\text{sat}}\sigma_{\text{halo}}$, where σ_{halo} is the velocity dispersion of the dark matter halos. In total, we use an HOD model with 9 free parameters, which we list in Table 1. We note that this is similar to the HOD model used in Zhai et al. (2022).

From the HOD galaxy catalog in a $1 (h^{-1}\text{Gpc})^3$ box, we construct a CMASS-like galaxy catalog by applying the survey geometry and observational systematics. We first remap the simulation box to a cuboid volume with dimensions $1.414 \times 1.224 \times 0.5773 (h^{-1}\text{Gpc})^3$ using the Carlson & White (2010) method, which is one-to-one volume preserving and keeps local structures intact. Moreover, it allows us to efficiently fit the CMASS survey geometry. After translating and rotating the cuboid, we cut

Table 1. Parameters of our forward model and their priors.

name	description	prior
Cosmological parameters		
Ω_m	matter energy density	$\mathcal{U}(0.1, 0.5)$
Ω_b	baryon energy density	$\mathcal{U}(0.03, 0.07)$
h	dimensionless Hubble constant	$\mathcal{U}(0.5, 0.9)$
n_s	spectral index of the primordial power spectrum	$\mathcal{U}(0.8, 1.2)$
σ_8	amplitude of matter fluctuations on $8h^{-1}\text{Mpc}$ scales	$\mathcal{U}(0.6, 1.0)$
Halo occupation parameters		
$\log M_{\min}$	characteristic mass scale for halos to host a central galaxy	$\mathcal{U}(12., 14.)$
$\sigma_{\log M}$	scatter of halo mass at fixed galaxy luminosity	$\mathcal{U}(0.1, 0.6)$
$\log M_0$	minimum halo mass for halos to host a satellite galaxy	$\mathcal{U}(13., 15.)$
$\log M_1$	characteristic mass scale for halos to host a satellite galaxy	$\mathcal{U}(13., 15.)$
α	power-law index for the mass dependence of satellite occupation	$\mathcal{U}(0.0, 1.5)$
A_{bias}	assembly bias	$\mathcal{N}(0, 0.2)$ over $[-1, 1]$
η_{conc}	concentration bias of satellites	$\mathcal{U}(0.2, 2.0)$
η_{cen}	velocity bias of centrals	$\mathcal{U}(0.0, 0.7)$
η_{sat}	velocity bias of satellites	$\mathcal{U}(0.2, 2.0)$
Nuisance parameters		
A_{shot}	P_0 shot noise correction	$\mathcal{U}(-10^4, 10^4)$

out the survey geometry from it using MANGLE polygons (Swanson et al. 2008) from BOSS (Dawson et al. 2013) that includes the angular footprint of the survey as well as the veto mask, which includes masking for bright stars, centerpost, bad field, collision pen priority. We then trim the forward modeled galaxy catalog with the same $0.45 < z < 0.6$ range that we imposed on the observations. Lastly, we apply fiber collisions. We identify all pairs of galaxies within an angular scale of $62''$; then, for a randomly selected 60% of the pairs, we remove one of the galaxies from the sample.

In Figure 1, we present a comparison of the CMASS sample (top; blue) with a galaxy catalog generated from our forward model (bottom; orange). In the left and center panels, we present the 3D distribution of galaxies at two different viewing angle. For more comparisons of the 3D distributions, we refer readers to [Earth²](https://www.youtube.com/watch?v=PLQk8Faa2x0twK3fgs55ednnHD2vbIzo4z). In the right panels, we present the angular distribution of the galaxies. The forward modeled galaxy catalog has the same detailed angular footprint and redshift range as the CMASS sample with similar systematics.

3.2. Priors

² <https://youtube.com/playlist?list=PLQk8Faa2x0twK3fgs55ednnHD2vbIzo4z>

For the cosmological parameters, $\{\Omega_m, \Omega_b, h, n_s, \sigma_8\}$, we use uniform priors over the parameter ranges that fully encompass the *Planck* priors. We impose these priors by constructing the training data from QUIJOTE N -body simulations generated using cosmological parameters in an LHC configuration. For the HOD parameters, we choose conservative priors that can produce a broad range of galaxy populations. In particular, for the standard Z07 HOD parameters, $\{\log M_{\min}, \sigma_{\log M}, \log M_0, \log M_1, \alpha\}$, we choose their prior ranges so that a galaxy sample with a comparable number of galaxies as the observations can be forward modeled from any of the N -body simulations in the LHC by using a set of HOD parameter values within the priors. For instance, this led us to adopt broad conservative priors for $\log M_{\min}$ and $\sigma_{\log M}$. For assembly bias, we use a Gaussian prior centered at 0 with $\sigma = 0.2$ over the range $[-1, 1]$ for A_{bias} . Lastly, for concentration, central velocity, and satellite velocity bias we use uniform priors on $\eta_{\text{conc}}, \eta_{\text{cen}}, \text{and } \eta_{\text{sat}}$, respectively, with the same range as in Zhai et al. (2022). We list priors for our cosmological and HOD parameters in Table 1.

3.3. Summary Statistic

The SIMBIG framework enables us to derive robust cosmological constraints using any summary statistics of the observed galaxy distribution. In this work, however, our primary goal is to demonstrate and validate the SIMBIG framework so we use the galaxy power spectrum multipoles, $P_\ell(k)$, as our summary statistic. $P_\ell(k)$ is a standard cosmological observable that has been extensively analyzed in the literature. Later, we compare the constraints that we infer from our analysis to some of these previous works (Ivanov et al. 2020; Kobayashi et al. 2021).

For both observed and forward modeled galaxy samples, we use the Hand et al. (2017) P_ℓ estimator implemented in the `nbodykit` python package³ (Hand et al. 2018). The estimator is Fast Fourier Transform (FFT) based and uses FFTs with grid size $N_{\text{grid}} = 360$. The estimator accounts for the survey geometry using a random catalog that has the same radial and angular selection functions as the observed catalog but with a much larger number of objects ($>4,000,000$) with random angular and radial positions.

When measuring P_ℓ , we include FKP weights (Feldman et al. 1994) with $P_0 = 10^4$ to reduce the variance of the measured P_ℓ for a galaxy sample with non-uniform completeness. For the observed galaxy sample, we also include systematic weights. For galaxy i , we assign $w_{g,i} = w_{\text{sys},i} w_{\text{noz},i}$, where $w_{\text{sys},i}$ is an angular systematic weight based on stellar density and seeing conditions and $w_{\text{noz},i}$ is a redshift failure weight. We exclude weights for fiber collisions, which are typically included in other BOSS analyses (e.g. Beutler et al. 2017), because we include the effect in our forward model. We forward model fiber collisions because the standard weighting scheme does not accurately correct for them (Hahn et al. 2017a). Meanwhile, the other weights successfully account for their corresponding systematic effects so they are not included (Ross et al. 2012; Anderson et al. 2014).

For our summary statistic, we include the power spectrum monopole, quadrupole, and hexadecapole ($\ell = 0, 2$, and 4). Each multipole is measured with $\Delta k = 0.005$ and out to $k_{\text{max}} = 0.5 h/\text{Mpc}$

³ <https://nbodykit.readthedocs.io/en/latest/index.html>

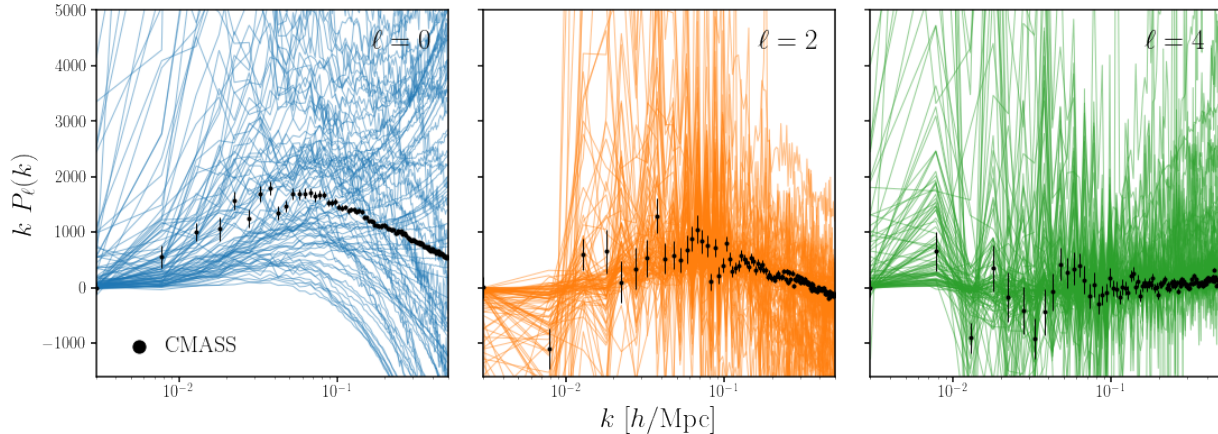


Figure 2. Power spectrum multipoles, $k P_\ell(k)$, of the simulated galaxy catalogs in our training dataset constructed from the QUIJOTE N -body simulations using our forward model. We randomly select 100 out of the 20,000 catalogs. We present the power spectrum monopole, quadrupole, hexadecapole ($\ell = 0, 2, 4$) in the left, center, and right panels. For reference, we include $k P_\ell(k)$ measured from the observed CMASS sample (black) with errorbars estimated from the TEST0 simulations.

with 100 k -bins. In addition to the power spectrum, we also include \bar{n}_g , the average galaxy number density. In total, our summary statistic has 301 elements.

3.4. Training Data

The SBI in SIMBIG requires a training dataset of $(\boldsymbol{\theta}', \mathbf{x}')$ pairs, where $\boldsymbol{\theta}'$ is a set of parameter values drawn from the prior and \mathbf{x}' is some observable — in our case P_ℓ and \bar{n}_g — forward modeled using $\boldsymbol{\theta}'$. To construct this training dataset, we begin with the 2000 QUIJOTE N -body simulations in the LHC configuration. For each simulation, we forward model 10 CMASS-like galaxy catalogs using unique HOD parameters randomly sampled from the prior. Afterwards, we measure $P_\ell(k)$ for all of the galaxy catalogs.

We supplement our training data with an additional parameter: A_{shot} , a nuisance parameter to marginalize over the residual shot noise contribution beyond the Poisson shot noise. We include A_{shot} mainly to be consistent with prior $P_\ell(k)$ analyses (Beutler et al. 2017; Ivanov et al. 2020; Kobayashi et al. 2021). In practice, we include A_{shot} for each P_0 by adding a constant sampled from a uniform prior: $A'_{\text{shot}} \sim \mathcal{U}(-10^4, 10^4)$. We use the same range for A_{shot} as Kobayashi et al. (2021).

In total, we construct a training dataset of 20,000 $(\boldsymbol{\theta}', P'_\ell)$ pairs. We present $k P_\ell(k)$ for a randomly selected subset of the training dataset in Figure 2. The left, center, and right panels present the monopole, quadrupole, and hexadecapole respectively. For reference, we include P_ℓ of the observed CMASS sample (black) with uncertainties estimated using the TEST0 simulations, which we describe later in Section 4.1. With our choice of conservative priors (Table 1), P_ℓ of the training dataset has a broad range that fully encompasses the observed P_ℓ .

3.5. Simulation-Based Inference with Normalizing Flows

Our main goal is to infer posterior distributions of cosmological parameters given a summary statistic of the observations: $p(\boldsymbol{\theta} | \mathbf{x})$. In the standard approach, the posterior is estimated using Markov Chain Monte Carlo (MCMC) sampling methods, where the posterior value of each sample is evaluated using Bayes’ rule based on the likelihood and prior. The likelihood is assumed to have a Gaussian functional form: $\ln p(\mathbf{x} | \boldsymbol{\theta}) = -\frac{1}{2}(\mathbf{x} - m(\boldsymbol{\theta}))^T \mathbf{C}^{-1}(\mathbf{x} - m(\boldsymbol{\theta}))$, where $m(\boldsymbol{\theta})$ is the theoretical model and \mathbf{C} is the covariance matrix of the observables. MCMC requires drawing a large number of samples from the posterior distribution, which precludes simulated forward models from being used for $m(\boldsymbol{\theta})$. As we discuss in Section 1, this dramatically restricts the observables and the physical scales that we can analyze. Furthermore, the Gaussianity of the likelihood breaks down on low signal-to-noise regimes and higher-order statistics (Scoccimarro 2000; Hahn et al. 2019).

SBI offers an alternative that allows us to exploit forward models and relaxes the assumptions on the form of the likelihood (Cranmer et al. 2020). In this work, we use an SBI method that uses a training dataset to estimate the posterior using density estimation (*e.g.* Alsing et al. 2018; Wong et al. 2020; Huppenkothen & Bachetti 2021; Zhang et al. 2021; Hahn & Melchior 2022). We use simulated $(\boldsymbol{\theta}', \mathbf{x}')$ pairs to train a neural density estimator with parameters ϕ : $q_\phi(\boldsymbol{\theta} | \mathbf{x}')$. For our density estimator we use “normalizing flow” models (Tabak & Vanden-Eijnden 2010; Tabak & Turner 2013) that use an invertible bijective transformation, f , to map a complex target distribution to a simple base distribution, $\pi(\mathbf{z})$, that is fast to evaluate. In our case, the target distribution is the posterior and we use a multivariate Gaussian for our base distribution. The transformation f is defined to be invertible and have a tractable Jacobian so that the target distribution can be evaluated from $\pi(\mathbf{z})$ by change of variables. Since $\pi(\mathbf{z})$ is easy to evaluate, we can also easily evaluate the target distribution. A (NN) is trained to obtain f , which provides an extremely flexible mapping from the base distribution. In this work, we use Masked Autoregressive Flow (MAF; Papamakarios et al. 2017) models implemented in the `sbi` Python package⁴ (Greenberg et al. 2019; Tejero-Cantero et al. 2020). MAF model stacks multiple Masked Autoencoder for Distribution Estimation (MADE; Germain et al. 2015) models to combine normalizing flows with an autoregressive design (Uribe et al. 2016) that is well-suited for estimating conditional probability distributions such as a posterior.

Our goal is to train a normalizing flow that best approximates the posterior: $p(\boldsymbol{\theta} | \mathbf{x}) \approx q_\phi(\boldsymbol{\theta} | \mathbf{x})$. First, we split the training data into a training and validation set with a 90/10 split. Then we minimize the KL divergence between $p(\boldsymbol{\theta}, \mathbf{x}) = p(\boldsymbol{\theta} | \mathbf{x})p(\mathbf{x})$ and $q_\phi(\boldsymbol{\theta} | \mathbf{x})p(\mathbf{x})$, by maximizing the total log-likelihood $\sum_i \log q_\phi(\boldsymbol{\theta}_i | \mathbf{x}_i)$ over training set. We use the ADAM optimizer (Kingma & Ba 2017) with a learning rate of 5×10^{-4} . We prevent overfitting by evaluating the total log-likelihood on the validation data at every training epoch and stop the training when the validation log-likelihood fails to increase after 20 epochs. We determine the architecture of our normalizing flow through experimentation. We train multiple flows with randomly selected architectures and examine their validation losses as a function of epoch to ensure they were appropriately trained. Afterwards, we select one of the normalizing flows based on validation loss. We note that flows with comparable validation losses infer

⁴ <https://github.com/mackelab/sbi/>

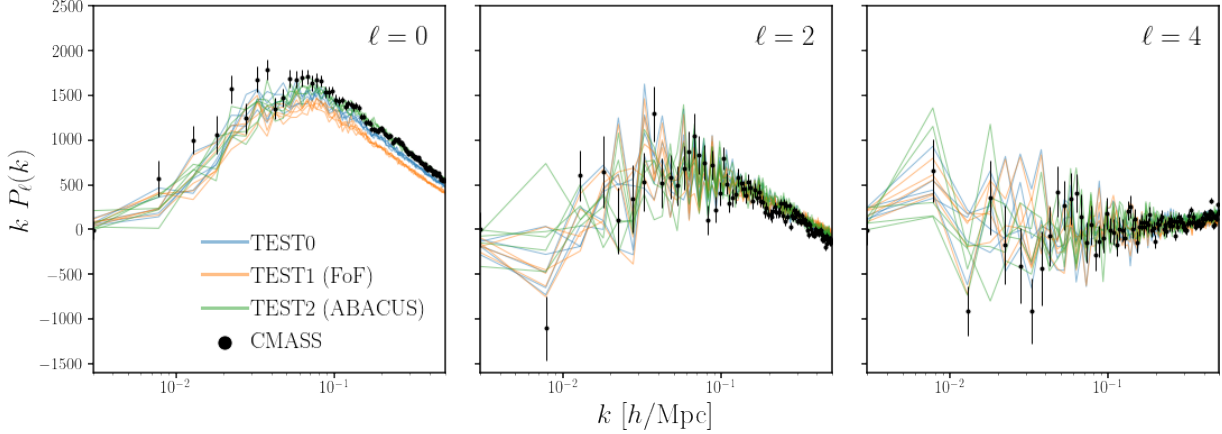


Figure 3. $k P_\ell(k)$ of the three sets of test simulations constructed to validate the SIMBIG framework. In each panel, we present $P_\ell(k)$ of 10 randomly selected simulations from TEST0 (blue), TEST1 (orange), and TEST2 (green). We present $\ell = 0, 2, 4$ in the left, center, and right panels. We include the $k P_\ell$ of CMASS galaxies (black) with uncertainties estimated using TEST0 for reference. We construct the test simulations with different sets of assumptions (N -body simulation, halo finder, HOD model) than the training set and thus there are noticeable differences among them. Overall, their P_ℓ that loosely agree with the CMASS P_ℓ .

overall consistent posteriors with $\lesssim 5\%$ variation. The flow we use has 6 MADE blocks, 9 hidden layers, and 186 units.

In $q_\phi(\boldsymbol{\theta} | \boldsymbol{x})$, $\boldsymbol{\theta}$ represents the 15 cosmological, HOD, and nuisance parameters and \boldsymbol{x} represents the 301 element summary statistic, $P_\ell(k)$ and \bar{n}_g . In principle, we can compress \boldsymbol{x} to reduce the dimensionality of the posterior. A variety of compression schemes can be used in conjunction with SBI. Alsing et al. (2018) and Charnock et al. (2018), for example, proposed compression schemes that maximize the Fisher information. These schemes require derivatives of the summary statistic with respect to the parameters to calculate the Fisher matrix. In our case, we use the QUIJOTE simulations in an LHC so we do not have access to derivatives with respect to cosmological parameters. An alternative compression scheme would be to train a NN that takes in the summary statistics as input and predicts the parameters. The predicted parameters would serve as the compressed summary statistic. We use this regression network to compress \boldsymbol{x} and conduct SBI on the compressed statistics. For our P_ℓ analysis, we find no significant difference between using the full versus compressed \boldsymbol{x} . We therefore use the full summary statistic in $q_\phi(\boldsymbol{\theta} | \boldsymbol{x})$ to infer the posteriors.

4. TEST SIMULATION SUITES

In this work we validate the SIMBIG framework and demonstrate that we can use it to infer accurate posteriors. One way to validate our posteriors is to compare them to previous constraints in the literature. We do this in H22a and later in Section 5. However, a more rigorous validation of SIMBIG is to demonstrate that we can infer accurate and unbiased parameter constraints for a suite of realistic test simulations that make different assumptions than our training set. In this section, we describe how we construct three different sets of test simulations: two using QUIJOTE and a third using the ABACUSSUMMIT N -body simulations (Maksimova et al. 2021).

4.1. QUIJOTE Test Simulations

Our goal for the test simulations is to construct galaxy samples that reflect the observed CMASS galaxies and are not part of our training data. For the first set of test simulations, we use the same forward model as our training data. However, instead of using the N -body simulations from the QUIJOTE LHC set, we use a different set of 100 independent QUIJOTE simulations run at the fiducial cosmology ($\Omega_m = 0.3175, \Omega_b = 0.049, h = 0.6711, n_s = 0.9624, \sigma_8 = 0.834$). The fiducial simulations have the same properties (*e.g.* volume, resolution) as the LHC simulations other than cosmology. We also sample HOD parameters from a narrower distribution of HOD parameters than the prior (Section 3.2). For the Z07 HOD parameters, we center the range around the best-fit HOD parameter values from Reid et al. (2014) with widths 0.058, 0.12, 0.26, 0.12, 0.36 for $\log M_{\min}, \sigma_{\log M}, \log M_0, \log M_1, \alpha$, respectively. We sample $A_{\text{bias}} \sim \mathcal{N}(0., 0.02)$, $\eta_{\text{conc}} \sim \mathcal{U}(0.9, 1.1)$, $\eta_{\text{cen}} \sim \mathcal{U}(0., 0.1)$, and $\eta_{\text{sat}} \sim \mathcal{U}(0.9, 1.1)$. The rest of our forward model (volume remapping, survey geometry, systematics) is applied in the same way as our training data. We use 5 different HOD parameter values per N -body simulation for a total of 500 test galaxy catalogs. We refer these test simulations as **TEST0**.

For the second set, we again construct our test galaxy samples from the QUIJOTE fiducial N -body simulations but using a different halo finder and HOD model. Instead of the ROCKSTAR halo finder we use halo catalogs constructed using the Friend-of-Friend (FoF) algorithm (Davis et al. 1985) with the linking length parameter set to $b = 0.2$. Furthermore, instead of the HOD model with assembly, concentration, and velocity biases we use the Z07 HOD model with no assembly, concentration, or satellite velocity bias. We include central velocity bias because the halo velocities in FoF halo catalogs correspond to the bulk velocity of the dark matter particles in the halo rather than the velocity of the central density peak of the halo, which better corresponds to the central galaxy velocity (Knebe et al. 2011; Behroozi et al. 2013). If we ignore this discrepancy, we produce an imprint of Fingers-of-God (FoG) on the power spectrum quadrupole that significantly deviates from observations. We sample 5 HOD parameters for each N -body simulation using the same range as **TEST0** for the Z07 HOD parameters and use fixed $\eta_{\text{cen}} = 0.2$. We refer the second set of 500 test simulations as **TEST1**.

4.2. ABACUS Test Simulations

In addition to the QUIJOTE based test simulations above, we construct a third, and most stringent, set of test simulations designed to test the assumptions in our N -body simulations and halo finder. We build the test simulations using the ABACUSSUMMIT N -body simulation (Maksimova et al. 2021) and the COMPASO halo finder (Hadzhiyska et al. 2022). ABACUSSUMMIT is a suite of large, high-accuracy N -body simulations constructed using the ABACUS code (Garrison et al. 2018, 2021). For the test simulations, we use 25 simulations in the “base” configuration out of the 150 simulations at 97 different cosmologies in the suite. The ABACUSSUMMIT simulations contain 6912^3 particles in a $(2 h^{-1} \text{Gpc})^3$ volume box and have significantly higher resolution than QUIJOTE.

From ABACUSSUMMIT, we use halo catalogs generated using COMPASO, a specialized spherical overdensity based halo finder. COMPASO improves halo deblending from spherical overdensity algorithms by considering the tidal radius around smaller halos before halo assignment. It also improves known limitation in identifying halos close to the center of mass of larger halos. COMPASO also uti-

lizes a post-processing (Bose et al. 2022) step to remove over-deblended halos and merge physically associated halos that have merged and then physically separated. This halo finder has been used with HOD models to accurately fit observed galaxy clustering (*e.g.* Yuan et al. 2022).

We use halo catalogs from the simulations of the ABACUSSUMMIT base configuration. We divide each halo catalog into 8 catalogs in $(1 h^{-1}\text{Gpc})^3$ volume boxes. Afterwards, we construct galaxy catalogs with the same HOD model as our training data with 5 sets of HOD parameter values per simulation sampled from the same parameter ranges as TEST0. We apply the rest of our forward model in the same way as our training data to construct realistic CMASS-like test galaxy catalogs. We refer the third set of 1000 test simulations as TEST2.

In Figure 3, we present $k P_\ell(k)$ of the TEST0 (blue), TEST1 (orange), and TEST2 (green) simulations that we use to test SIMBIG. We present 10 randomly selected test simulations from each suite and plot $\ell = 0, 2, 4$ in the left, center, and right panels. For reference, we present $k P_\ell(k)$ of CMASS galaxies in black with uncertainties estimated from the TEST0 simulations. Overall, the $k P_\ell$ among the test suite loosely agree with the observed P_ℓ . There are notable differences among them since we construct each of them using different forward models.

5. RESULTS

In Figure 4, we present the posterior distribution inferred from the CMASS P_ℓ with $k_{\text{max}} < 0.5 h/\text{Mpc}$ using SIMBIG. In the top panels, we present the posterior of the cosmological parameters. In the bottom panels, we present the posterior of the halo occupation and nuisance parameters. The diagonal panels present the one-dimensional marginalized posteriors; the other panels present marginalized posteriors of different parameter pairs. The contours represent the 68 and 95 percentiles and the range of the panel represents the prior range. We also list the 50, 16, and 84th percentile constraints on the parameters along the diagonal panels.

The SIMBIG posterior is inferred using mostly uniform priors (except A_{bias}). It, therefore, provides insights into which parameters are constrained by P_ℓ . We present and discuss the cosmological constraints in detail in H22a. Here, we focus on the halo occupation parameters. We derive particularly tight constraints on $\log M_{\text{min}}$ and η_{cen} . Based on the constraints, we find that CMASS central galaxies reside in halos with $M_h > 10^{13} M_\odot$. This is in good agreement with previous CMASS HOD constraints (Reid et al. 2014). Our constraints on the Z07 HOD parameters are also in good agreement with Kobayashi et al. (2021) HOD parameter constraints. Kobayashi et al. (2021) recently analyzed $P_\ell(k)$ using a halo power spectrum emulator with an analytic prescription for the Z07 HOD model.

Our posterior also provides insights into halo occupation beyond the Z07 model. For instance, we find a significantly non-zero central velocity bias. This suggests that there is a significant velocity offset between CMASS central galaxies and their halos, which is consistent with past studies (Guo et al. 2015; Yuan et al. 2020; Lange et al. 2021; Zhai et al. 2022). Meanwhile, we find little evidence for satellite velocity bias similar to Lange et al. (2021) and Zhai et al. (2022). We also do not find evidence of assembly bias: our posterior does not significantly constrain A_{bias} .

Next, we validate the accuracy of the posterior. We run the SIMBIG posterior estimator, q_ϕ , on each of the test simulations described in Section 4. In Figure 5, we present the posteriors of (Ω_m, σ_8) for a randomly selected subset of the test simulations. We present posteriors for TEST0, TEST1, and

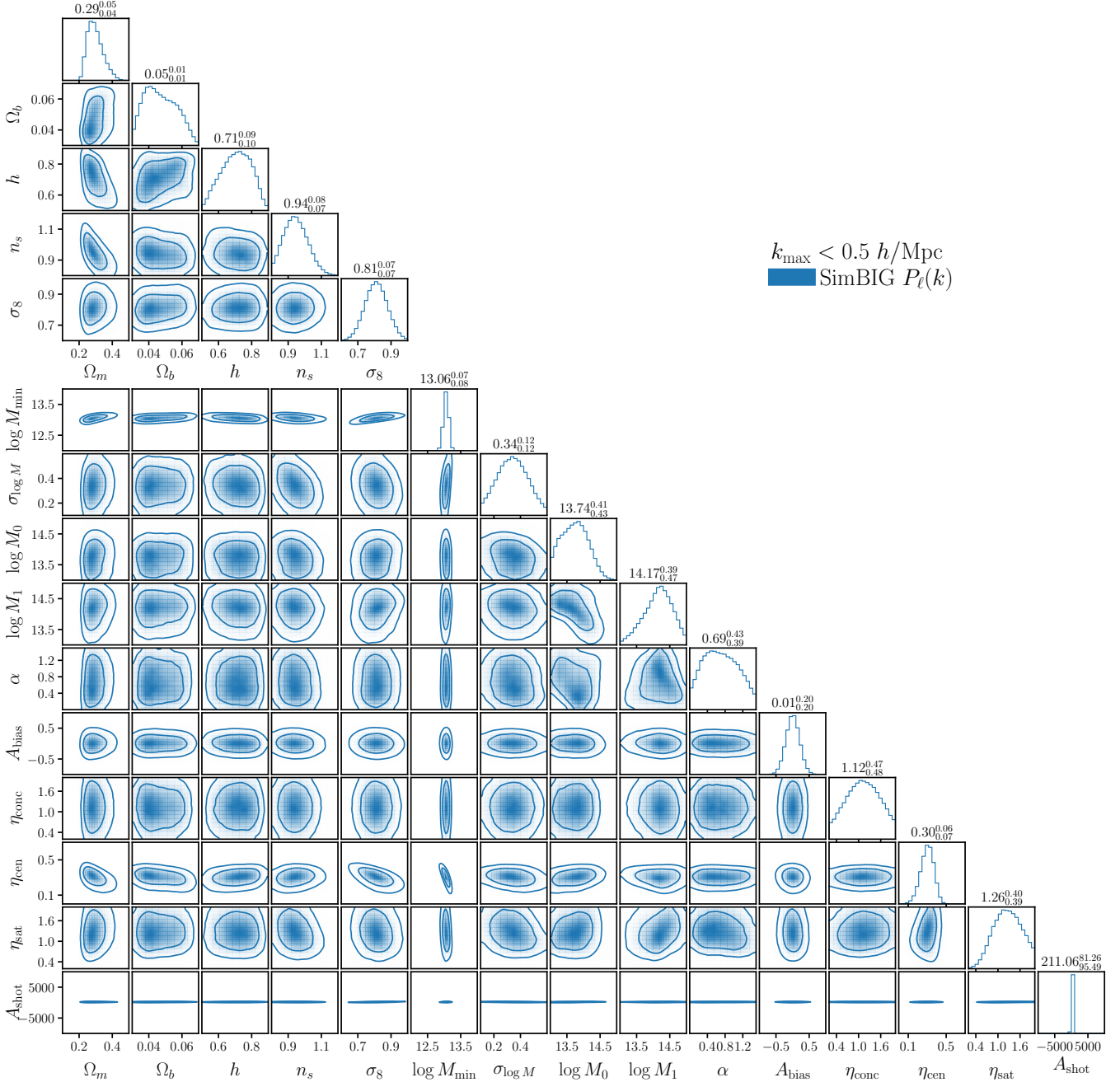


Figure 4. Posterior distribution of all parameters inferred from the BOSS CMASS $P_\ell(k)$ analysis to $k_{\text{max}} < 0.5 h/\text{Mpc}$ using SIMBIG. In the top set of panels, we present the cosmological parameters. In the bottom, we present the halo occupation and nuisance parameters. The range of the panels represent the prior range in Table 1. Among the halo occupation parameters, the posterior significantly constrains $\log M_{\text{min}}$ and η_{cen} . Among the cosmological parameters, the posterior significantly constrains Ω_m and σ_8 .

TEST2 simulations in the top, center, and bottom panels. The contours represent the 68 and 95 percentiles of the posteriors. In each panel, we mark the true (Ω_m, σ_8) value of the test simulation (black x). Each test simulation is a unique realization of a CMASS-like galaxy catalog subject to

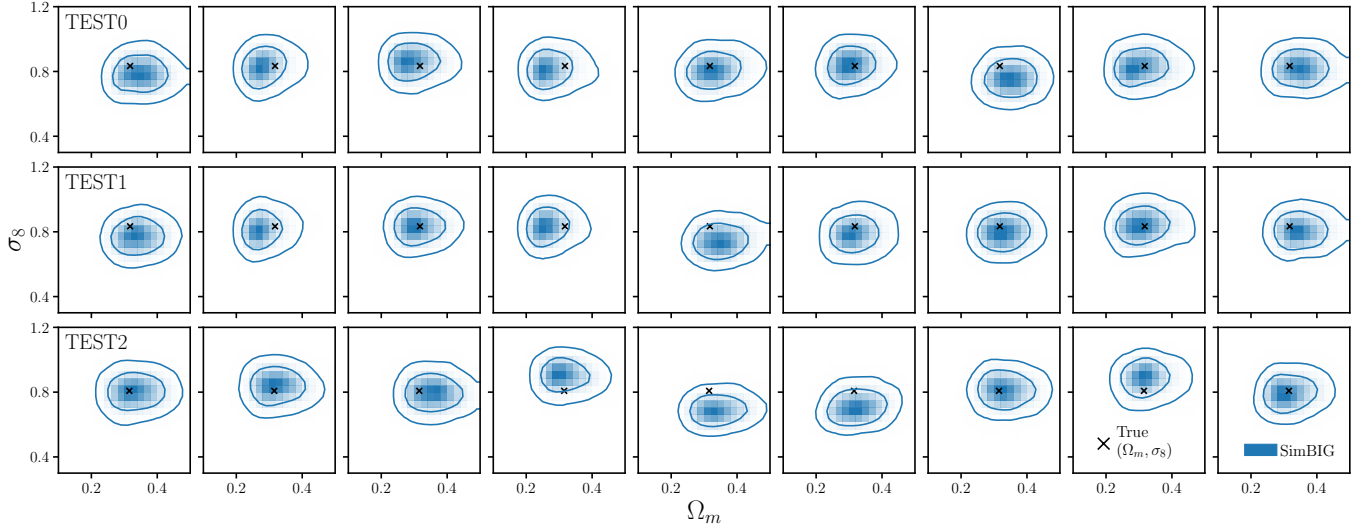


Figure 5. Posteriors of (Ω_m, σ_8) inferred using SIMBIG for a random subset of the **TEST0** (top), **TEST1** (center), and **TEST2** (bottom) simulations. We mark the 68 and 84 percentiles of the posteriors with the contours. We also include the true (Ω_m, σ_8) of the test simulations in each panel (black \times). The comparison between the posteriors and the true parameter values qualitatively show good statistical agreement for each of the test simulations.

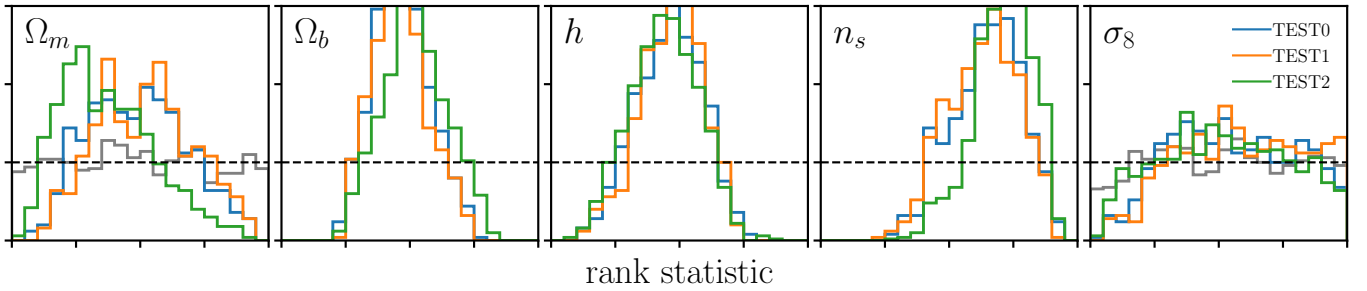


Figure 6. SBC validation of the posteriors estimated using SIMBIG for test simulations. We present the distribution of the rank statistics, which are derived by comparing the true parameter values to the inferred marginalized 1D posteriors. In general, for an accurate estimate of the true posterior, the rank statistic would be uniformly distributed (black dashed). In our case, since we use test simulations evaluated at fiducial cosmologies, our priors impose a \cap -shape, especially for Ω_b , h , and n_s . We include the expected rank distribution for an accurate estimate of the true posterior for Ω_m and σ_8 (gray). Since the distributions for Ω_m and σ_8 have symmetric \cap -shape with respect to this expected distribution, SIMBIG posteriors are unbiased but broader than the true posteriors. The rank distributions for different test simulations show an overall good agreement and, thus, illustrate that the SIMBIG approach is robust to the choices in our forward model. Overall, *the SIMBIG produces unbiased and conservative posteriors for Ω_m and σ_8 .*

cosmic and statistical variance. We, therefore, do not expect the true (Ω_m, σ_8) value to lie at the center of each of the posteriors. Instead, we note that for the majority of the randomly selected test simulations, the true parameter values lie within the 68 and 95 percentiles SIMBIG posteriors.

We assess the accuracy and precision of the SIMBIG more quantitatively using simulation-based calibration (SBC; Talts et al. 2020). For each test simulation and each cosmological parameter, we calculate the rank of the true parameter value within the marginalized 1D SIMBIG posterior. In practice, for each parameter, θ , and test simulation j , we calculate the rank of $\theta_{j,\text{test}}$ within the θ values sampled from the posterior estimate: $\{\theta'_1, \theta'_2, \dots, \theta'_N\} \sim q_\phi(\theta | \mathbf{x}_{j,\text{test}})$. For instance, $\theta_{j,\text{test}}$ would have rank 1 if $\theta_{j,\text{test}} < \theta'_1, \theta'_2, \dots, \theta'_N$ or rank N if $\theta_{j,\text{test}} > \theta'_1, \theta'_2, \dots, \theta'_N$. We then compile the ranks for all of the test simulations in each suite and plot their histogram. This distribution and variations of it (conditional coverage) are common diagnostics for posterior estimates (*e.g.* Green & Gair 2020; Hahn & Melchior 2022; Lemos et al. 2022). If we estimate the true posterior exactly, the rank statistics would be distributed uniformly. If instead the rank statistics have a U-shaped distribution, the true parameter values are more often at the lowest and highest ranks, so the posterior estimates are narrower than the true posteriors. If the distribution has a \cap -shape, then the posterior estimates are broader than the true posteriors. An asymmetric distribution implies that the posterior estimates are biased.

In Figure 6, we present the distribution of rank statistics for the cosmological parameters in all of the test simulations. In each panel, we present the distributions for the TEST0 (blue), TEST1 (orange), and TEST2 (green) simulations. Overall, the distributions have a \cap -shape and are symmetric. The \cap -shape is in part due to the prior range on the cosmological parameters and the fact that our test simulations are constructed at a fiducial cosmology. This is especially the case for Ω_b , h , and n_s whose prior ranges truncate the SIMBIG posterior constraints (Figure 4). The true parameter values of the test simulations are at fiducial values near the center of the prior: $\Omega_b^{\text{fid}}, h^{\text{fid}}, n_s^{\text{fid}} = 0.0490, 0.6711, 0.9624$ for TEST0 and TEST1 and $0.0493, 0.6736, 0.9649$ for TEST2. Hence, since the tails of the likelihood are truncated by the prior, the true parameter values will have more central ranks within the marginalized posterior. Galaxy clustering, however, does not place strong constraints on these parameters. Previous works (Ivanov et al. 2020; Kobayashi et al. 2021) typically use priors from either big bang nucleosynthesis or CMB constraints for Ω_b and n_s . We, therefore, focus on Ω_m and σ_8 , the cosmological parameter most significantly constrained by galaxy clustering alone.

The prior range also affects the rank statistic distribution of σ_8 . The σ_8 posterior is within the prior but has a comparable width to the prior range (Figure 4). To estimate the effect of the prior range on our SBC for σ_8 , we consider a simplified scenario assuming a fixed likelihood. We draw 10,000 samples from the marginalized σ_8 posterior for an arbitrary TEST0 simulation: $\sigma'_8 \sim q_\phi(\sigma_8 | \mathbf{x}_{\text{test}})$. The TEST0 simulations have a σ_8 value of σ_8^{fid} . For each sample, σ'_8 , we shift the posterior by $\sigma_8^{\text{fid}} - \sigma'_8$. Since this shift may cause the posterior to go beyond the σ_8 prior of our analysis, we impose the σ_8 prior range on the shifted posterior. Afterward, we calculate the rank of the sample within the truncated and shifted posterior. We include the rank distribution we obtain from this procedure (gray) for both Ω_m and σ_8 in Figure 6. The suppression of the σ_8 rank distributions at low ranks is due to the prior range. Once we take the prior range into account, the σ_8 rank distributions for TEST0, TEST1, and TEST2 are in good agreement with the expected rank distribution for an accurate estimate of the true posterior. We therefore conclude that the SIMBIG posterior of σ_8 is unbiased and slightly conservative.

For Ω_m , the posterior is well within the prior so the prior range does not have a significant impact on its rank statistic distribution (see gray distribution in left most panel of Figure 6). Since the prior range does not fully account for the \cap -shape, this implies that the SIMBIG posteriors of Ω_m is significantly broader than the true posteriors. This is due to the fact that we use a limited number of training simulations. Although we construct 20,000 training simulations, they only sample 2,000 different cosmologies. Consequently, our estimate of the KL divergence between the normalizing flow and the true posterior, which we minimize to train the flow, is intrinsically noisy. So the divergence cannot be further minimized to better estimate the posterior. Despite being conservative, the rank statistic distributions are symmetric so the SIMBIG posterior of Ω_m is unbiased.

Figure 6 also reveals the consistency among the rank statistics distributions for the different test simulations. We use different forward models to construct TEST1 and TEST2 than the training data. The accuracy and precision of the SIMBIG posteriors are not impacted by these differences and, thus, demonstrates the robustness of our SIMBIG approach. We therefore conclude that *we can use SIMBIG to infer unbiased and conservative posteriors from $P_\ell(k)$ to $k_{\max} = 0.5 h/\text{Mpc}$.*

6. DISCUSSION

Now that we have validated the robustness of the SIMBIG posteriors using the test simulations, we discuss other caveats of the SIMBIG framework as well as improvements for future applications. In particular, we focus on the forward model. SBI, and thus SIMBIG, relies on a forward model that can accurately model the observables.

6.1. Forward Model

Our forward model consists of the QUIJOTE N -body simulations, the ROCKSTAR halo finder, an HOD model, and the model for BOSS CMASS-SGC survey realism. In this section we examine each aspects of our forward model.

6.1.1. N -body Simulation

We use high resolution QUIJOTE N -body simulations to model the clustering of matter. Full N -body simulations more accurately model non-linear matter clustering than more approximate methods such as particle mesh scheme (*e.g.* Feng et al. 2016). While the accuracy of N -body simulations depends on their resolution, the matter clustering of QUIJOTE simulations are converged at $k \sim 0.5 h/\text{Mpc}$ even for simulations with lower resolution than our 1024^3 resolution (Villaescusa-Navarro et al. 2020). The QUIJOTE simulations are run using the TreePM GADGET-III code. We do not expect the choice of N -body code to impact our results as different N -body codes produce highly consistent matter clustering (Shao et al. 2022).

We also note that the QUIJOTE N -body simulations do not include baryonic effects. Feedback from active galactic nuclei (AGN), for instance, can impact the matter distribution at cosmological distance (van Daalen et al. 2011; Vogelsberger et al. 2014; Hellwing et al. 2016; Peters et al. 2018; Springel et al. 2018; Chisari et al. 2018; Barreira et al. 2019; Foreman et al. 2019; van Daalen et al. 2020). The impact, however, is mainly found on very small scales and is a subpercent effect on the power spectrum at $k < 0.5 h/\text{Mpc}$. We note that other baryonic processes also take effect on smaller

scales than our analysis (*e.g.* White 2004; Zhan & Knox 2004; Jing et al. 2006; Rudd et al. 2008; Harnois-Déraps et al. 2015). We, therefore, do not expect baryonic effects to have a significant impact on our parameter constraints.

6.1.2. Halo Occupation

From the matter distribution, we simulate the galaxy distribution using the ROCKSTAR halo finder and an HOD model. ROCKSTAR is a phase-space based halo finder designed to maximize halo consistency across time-steps. It first selects particle groups using a 3D FoF algorithm with a large linking length, then builds a hierarchy of FoF subgroups in phase space by progressively and adaptively reducing the linking length. Afterwards, ROCKSTAR converts the FoF subgroups into halos starting from the deepest level of the hierarchy. According to the Knebe et al. (2011) comparison of 18 different halo finders using test halo simulations, phase-space halo finders like ROCKSTAR can accurately resolve the spatial location of halos as well as the substructure near the center of halos. Furthermore, ROCKSTAR can accurately resolve substructure containing 10-20 particles. Knebe et al. (2011) found that phase-space halo finders are in good agreement for halo properties. They, however, found significant discrepancies among the halo finders on subhalo properties. In our forward model, we only use central halos so we are not impacted by the lack of convergence in subhalo properties among halo finders.

The HOD model that we use to populate halos with galaxies includes assembly bias, concentration, central velocity, and satellite velocity biases. This is a state-of-the-art HOD model that provides a highly flexible framework for populating galaxies in halos. As we demonstrate above, it is sufficiently flexible to reproduce the observations for $P_\ell(k)$. However, this may not be the case for summary statistics beyond the power spectrum that may be more sensitive to the limitations of the HOD model. Whether the HOD model is sufficiently descriptive must be determined for each summary statistics.

6.1.3. Survey Realism

The last step of our forward model is to apply the survey realism of the BOSS CMASS SGC sample. From the galaxy distribution in a $(1 h^{-1}\text{Gpc})^3$ box, we cut out the exact survey volume of the CMASS sample. One detail omitted in this procedure is the redshift evolution of the galaxy distribution. Our galaxy distribution is constructed at a single $z = 0.5$ snapshot. However, we do not expect a significant redshift dependence in the galaxy distribution or the underlying matter distribution over our narrow redshift range, $0.45 < z < 0.6$. We also do not expect a significant redshift dependence on the HOD, since CMASS galaxies were selected to have a roughly constant mass limit throughout the redshift range.

After we apply the survey geometry, we impose observational systematics. A key systematic that we include in our forward model is the effect of fiber collisions. For our forward model, we “collide” galaxies by randomly select 60% of galaxy pairs that have angular separation less than $62''$ and removing one of the galaxies in the selected pair. In this implementation, fiber collisions occur uniformly over the survey footprint. In principle, fiber collisions in SDSS-III depend on the tiling scheme used and are not uniformly distributed (Dawson et al. 2013). Regions observed by overlapping tiles

have lower fiber collision rates than regions observed by a single tile (Guo et al. 2012). Hahn et al. (2017a) examined the impact of fiber collisions on $P_\ell(k)$ using two sets of simulations Nseries and QPM (White et al. 2014). Nseries applied fiber collisions using the full SDSS tiling scheme while QPM applied fiber collisions in the same fashion as our forward model. Hahn et al. (2017a) examined the impact of fiber collisions on P_ℓ for both of the simulations and found little difference. We, therefore, conclude that the angular dependence of fiber collisions is not a significant effect for our analysis.

Another observational effect that we do not include in our forward model is incompleteness. The CMASS sample does not include all galaxies within its angular footprint that pass the target selection criteria. There is incompleteness due to imaging systematics. CMASS galaxies are selected for observation using the SDSS imaging data. Systematics in the imaging, such as seeing, sky background, airmass, galactic extinction, have significant correlations with the number density of galaxies. There is also incompleteness due to failures in measuring an accurate redshift. Redshift failures occur more frequently for galaxy spectra measured using a fiber near the edge of the focal plane. Ross et al. (2012) and Ross et al. (2017) model these effects and derive weights that can accurately correct for them. We opt to use these completeness weights since they have been demonstrated to sufficiently correct for incompleteness in the two-point clustering. Yet they may not be sufficient for higher-order. We reserve a more detailed investigation of the impact of completeness to future work.

6.2. Outlook

In this work, we present the mock challenge validation framework and additional details of SIMBIG. We demonstrate that we can use SIMBIG to analyze the BOSS CMASS galaxy sample with P_ℓ as our summary statistics. This is only the first steps. The SIMBIG framework can be applied beyond the BOSS CMASS P_ℓ .

6.2.1. Beyond $P_\ell(k)$

In subsequent work, we will use SIMBIG to analyze summary statistics that forecasts show can significantly improve cosmological constraints over the power spectrum (Hahn & Villaescusa-Navarro 2021; Massara et al. 2022; Hou et al. 2022). We will analyze the BOSS galaxy bispectrum, the simplest statistic beyond P_ℓ that captures non-Gaussian galaxy clustering information (Hahn et al. in prep.). We will also analyze the marked power spectrum multipoles, which measures the two-point clustering statistics of a weighted galaxy field (Massara et al. in prep.). In another work, we will present constraints from the weighted skew spectra, which are simple and interpretable proxy statistics for the bispectrum (Hou, Moradinezhad et al. in prep.).

The SIMBIG framework also enables clustering analyses using more novel summary statistics. For instance, Eickenberg et al. (2022) recently demonstrated that 3D wavelet statistics can extract non-Gaussian information and significantly improve cosmological parameter constraints. We will present cosmological constraints from BOSS CMASS using wavelet statistics in Eickenberg, Regalado, et al. (in prep.). With SIMBIG we can analyze any summary statistic that can be measured in the observed galaxy distribution. Hence, we will also present constraints from summary statistics that compress the full BOSS CMASS galaxy field using convolutional and graph NNs (Lemos et al. in prep.).

6.2.2. Beyond BOSS CMASS

While all of the studies described above will analyze the BOSS CMASS sample, SIMBIG can be extended to upcoming and future surveys such as DESI, PFS, *Euclid*, and Roman. In particular, the DESI Bright Galaxy Survey (BGS; [Hahn et al. 2022a](#)) and PFS will provide high density samples ideal for SIMBIG-like analyses. BGS will observe a $r < 19.5$ magnitude-limited galaxy sample out to $z = 0.6$ over a $14,000 \text{ deg}^2$ angular footprint. It will also have a number density an order-of-magnitude higher than CMASS. Meanwhile, PFS will observe a high number density sample of emission line galaxies (ELGs) over the range $0.6 < z < 2.4$ over a $1,200 \text{ deg}^2$ angular footprint. In this work, we analyze the BOSS CMASS-SGC sample because of the volume and resolution limit of the QUIJOTE N -body simulations. Both BGS and PFS will cover substantially larger volumes. This will be a challenge in extending SIMBIG.

Fully spanning the BGS and PFS volume will require significantly larger simulations of 3 and $7 (h^{-1} \text{Gpc})^3$, respectively. Both BGS and PFS galaxy samples will also require significantly higher resolution than QUIJOTE. BGS will probe galaxies with stellar masses as low as $M_* \sim 10^7 M_\odot$. Meanwhile, ELGs can reside in low mass halos with $M_h \sim 10^{11} M_\odot$. Fortunately, new developments in computational techniques and ML will make it possible to construct larger and higher-resolution simulations. Approximate N -body schemes, such as particle mesh, are significantly improving in both accuracy and speed ([Feng et al. 2016](#); [Modi et al. 2021](#)). Their accuracy can also be enhanced using methods such as potential gradient descent ([Dai et al. 2020](#)).

Furthermore, ML methods have now firmly demonstrated that they can be used to efficiently construct accurate high-resolution simulations. [Schaurecker et al. \(2021\)](#), for example, showed that convolutional NN can be used to enhance low resolution N -body simulations to create super-resolution simulations that accurately reproduce the cluster of high resolution simulations. Along similar lines, [Alves de Oliveira et al. \(2020\)](#) and [Jamieson et al. \(2022\)](#) successfully constructed accurate emulators for high resolution simulations. These ML methods would enable us to leverage a limited number of simulations, used for training, to construct a large set of emulated simulations with comparable accuracy.

6.2.3. Beyond Λ CDM

We assume a Λ CDM cosmology for the cosmological constraints that we present in this work. The subsequent SIMBIG papers will also focus on Λ CDM cosmological constraints. With SIMBIG, however, we can incorporate cosmological models beyond Λ CDM. We can expand the cosmological parameters to include, for instance, the dark energy equation of state, massive neutrinos, or primordial non-Gaussianity by replacing the N -body simulations. All other aspect of the SIMBIG forward modeling pipeline does not depend on cosmology.

We expect the SIMBIG approach to be especially effective for measuring the total mass of neutrinos, M_ν . Recent forecasts illustrate that higher-order statistics can tightly constrain M_ν (*e.g.* [Hahn et al. 2020](#); [Massara et al. 2020](#); [Hahn & Villaescusa-Navarro 2021](#)). Furthermore, massive neutrinos suppress the growth of structure on small scales below their free-streaming scale so M_ν analyses

require careful treatment of any systematics that affect small scale clustering. SIMBIG provides a comprehensive framework for exploiting higher-order galaxy clustering down to small scales.

6.2.4. *Beyond the HOD*

A major ingredient of our forward model is the HOD, which provides the mapping between the dark matter halos and galaxy distributions. Halo occupation in current HOD models only depends on a few halo properties (*e.g.* halo mass). There is, however, growing evidence that the galaxy-halo connection depends significantly on the halos’ detailed assembly history (*e.g.* Gao et al. 2005; Wechsler et al. 2006; Gao & White 2007; Zentner 2007; Dalal et al. 2008; Lacerna & Padilla 2011; Miyatake et al. 2016; More et al. 2016; Zentner et al. 2016; Lehmann et al. 2017; Vakili & Hahn 2019; Hadzhiyska et al. 2021; Hadzhiyska et al. 2022). This effect is commonly referred to as “halo assembly bias” and we include it in our HOD model by include a dependence of the galaxy occupation on halo concentration. Although we do not find significant constraints on assembly bias (A_{bias}), this is not evidence of the lack of assembly bias. Assembly bias may yet have a significant impact on more precise galaxy clustering measurements. It may also impact summary statistics beyond P_ℓ . Moreover, our decorated HOD implementation may not accurately model the effect of assembly bias in detail.

Fortunately, there are various avenues for improving halo occupation models. For instance, Delgado et al. (2022) demonstrated that halo occupation can be more accurately predicted if information on local environmental overdensity and shear is included. Jespersen et al. (2022) similarly find that galaxy properties, and thus occupation, can be more accurately predicted by including information on halo assembly history. Moreover, halo occupation models encapsulate only a particular aspect of galaxy formation and evolution. Better understanding of galaxies will, therefore, improve halo occupation models. We emphasize that SIMBIG, with its modular forward modeling approach, provides an ideal cosmological analysis framework for incorporating such improved models.

Along these lines, the SIMBIG approach also provides steps towards more fully extracting the cosmological information from galaxies and their detailed properties. Villaescusa-Navarro et al. (2022) controversially claimed that there may be significant cosmological information even in a single galaxy. The precision for which we can measure the detailed properties of galaxies such as stellar mass and star formation rate will pose major challenges for any cosmological inference with a single galaxy. However, cosmological inference may be possible with statistically powerful galaxy samples with measured galaxy properties. For instance, the probabilistic value-added BGS catalog (Hahn et al. 2022b) will provide stellar mass, star formation rate, and stellar metallicity measurements of 15 million BGS galaxies.

We can in principle replace the halo occupation model in SIMBIG with galaxy formation models that predict galaxy properties, such as semi-analytic models or emulators of cosmological hydrodynamical simulations (see Somerville & Davé 2015, for a review). Then, with the SBI framework of SIMBIG, we can conduct robust cosmological inference using summary statistics that take advantage of galaxy properties. Ultimately, SIMBIG provides a framework for maximally extracting cosmological information from spectroscopic galaxy surveys.

7. SUMMARY

We present SIMBIG, a forward modeling framework for constraining cosmological parameters from galaxy clustering using simulation-based inference. SIMBIG enables robust analysis of galaxy clustering on non-linear scales with higher-order statistics, that accounts for observational systematics. As a demonstration, we use SIMBIG to analyze $P_\ell(k)$ of the SDSS-III BOSS CMASS SGC galaxy sample to $k_{\text{max}} = 0.5 h/\text{Mpc}$. In an accompanying paper (Hahn et al. 2022), we present the cosmological constraints in detail. In this work, we describe our forward model and present the mock challenge for validating our cosmological parameter constraints using a suite of test simulations.

Our forward model is designed to model the observed galaxies in the CMASS SGC sample. It is based on 2000 high-resolution QUIJOTE N -body simulations that are evaluated at different cosmologies arranged in a latin hypercube configuration to impose uniform priors. From the N -body simulations we construct galaxy simulations by first identifying dark matter halos using ROCKSTAR and then populating the halos using a flexible HOD model. Our HOD model extends the standard Zheng et al. (2007) model by including assembly, concentration, central velocity, and satellite velocity biases. As the last step of our forward model, we apply full survey realism onto the galaxy simulations. We model the BOSS CMASS-SGC survey geometry and apply angular masking as well as fiber collisions. In total we construct 20,000 forward model galaxy catalogs. We measure $P_\ell(k)$ of these catalogs and use the measurements to train our normalizing flow and conduct SBI.

For our mock challenge, we construct three sets of test simulations: TEST0, TEST1, and TEST2. TEST0 is constructed using the same forward model as the simulations used for SBI but with QUIJOTE simulations at a fiducial cosmology. TEST1 is constructed using a different forward model. We use the same N -body simulations but with a different halo finder (FoF) and HOD model. TEST1 is also constructed using a different forward model, where we use a different N -body simulation (ABACUSUMMIT) and a different halo finder (COMPASO). To validate SIMBIG, we infer posteriors for $P_\ell(k)$ measured for each of the test simulations. We then use the true cosmologies of the test simulations to assess the accuracy and precision of the SIMBIG posteriors.

Based on the SIMBIG posteriors and the mock challenge, we find the following results.

- From our P_ℓ SIMBIG analysis, we derive constraints on cosmological, HOD, and nuisance parameters. Among the HOD parameters, our constraints on the Z07 model parameters are in good agreement with previous works (Reid et al. 2014; Kobayashi et al. 2021). Our constraints on central and satellite velocity biases are also in good agreement with the literature (Guo et al. 2015; Yuan et al. 2020; Lange et al. 2021; Zhai et al. 2022). We do not significantly constrain assembly bias. For our cosmological constraints, we refer readers to H22a.
- Based on the mock challenge, we demonstrate that SIMBIG posteriors are unbiased. SIMBIG infers statistically unbiased posteriors of the cosmological parameters for the test simulations. Since the test simulations are constructed using significantly different forward models, this is a clear demonstrate of the robustness of SIMBIG.
- We also find that the SIMBIG posteriors are conservative. We derive broader posteriors than the true posteriors for the test simulations. This is due to the limited number of N -body

simulations used in our SBI. Our training dataset is based on only 2,000 different cosmological parameters. Additional simulations will improve the accuracy of the SIMBIG posteriors.

Overall, the mock challenge results demonstrate that we can use SIMBIG to robustly and accurately analyze galaxy clustering. Although our posteriors are conservative, because we extract cosmological information on small scales inaccessible with perturbation theory analyses, our constraints are competitive.

In this work and [Hahn et al. \(2022\)](#), we analyze $P_\ell(k)$ for the primary purpose of demonstrating the SIMBIG framework. Our $P_\ell(k)$ analysis only takes advantage of Gaussian cosmological information down to small scales. Forecasts suggest that significant amount of non-Gaussian cosmological information can be extracted using higher-order statistics. In subsequent work, we will use SIMBIG to analyze observables beyond P_ℓ , including the bispectrum, marked power spectrum, skew spectra, wavelet statistics, and field-level statistics.

The SIMBIG framework is currently designed to analyze the BOSS CMASS galaxies. However, SIMBIG provides a highly modular framework that can be used to analyze upcoming galaxy surveys. The SIMBIG forward model can be enhanced, for instance, by replacing the QUIJOTE simulations with higher resolution or larger simulations. New halo occupation models being developed in the literature can also improve how we populate the forward model with galaxies. New applications of ML also offer many opportunities to improve SIMBIG by exploiting fast emulation or super-resolution. SIMBIG will be particularly effective for analyzing the upcoming DESI BGS and PFS that will provide high density galaxy samples over unprecedented cosmic volumes.

ACKNOWLEDGEMENTS

It's a pleasure to thank Mikhail M. Ivanov and Yosuke Kobayashi for providing us with the posteriors used for comparison. We also thank Peter Melchior, Uroš Seljak, David Spergel, Licia Verde, and Benjamin D. Wandelt for valuable discussions. This work was supported by the AI Accelerator program of the Schmidt Futures Foundation. JH has received funding from the European Union's Horizon 2020 research and innovation program under the Marie Skłodowska-Curie grant agreement No 101025187. AMD acknowledges funding from Tomalla Foundation for Research in Gravity and Boninchi Foundation.

REFERENCES

- | | |
|---|--|
| <p>Abareshi, B., Aguilar, J., Ahlen, S., et al. 2022, Overview of the Instrumentation for the Dark Energy Spectroscopic Instrument, doi: 10.48550/arXiv.2205.10939</p> <p>Alsing, J., Charnock, T., Feeney, S., & Wandelt, B. 2019, Monthly Notices of the Royal Astronomical Society, 488, 4440, doi: 10.1093/mnras/stz1960</p> | <p>Alsing, J., Wandelt, B., & Feeney, S. 2018, arXiv:1801.01497 [astro-ph]. https://arxiv.org/abs/1801.01497</p> <p>Alves de Oliveira, R., Li, Y., Villaescusa-Navarro, F., Ho, S., & Spergel, D. N. 2020, Fast and Accurate Non-Linear Predictions of Universes with Deep Learning</p> <p>Anderson, L., Aubourg, É., Bailey, S., et al. 2014, Monthly Notices of the Royal Astronomical Society, 441, 24, doi: 10.1093/mnras/stu523</p> |
|---|--|

- Barreira, A., Nelson, D., Pillepich, A., et al. 2019, *Monthly Notices of the Royal Astronomical Society*, 488, 2079, doi: [10.1093/mnras/stz1807](https://doi.org/10.1093/mnras/stz1807)
- Behroozi, P. S., Wechsler, R. H., & Wu, H.-Y. 2013, *The Astrophysical Journal*, 762, 109, doi: [10.1088/0004-637X/762/2/109](https://doi.org/10.1088/0004-637X/762/2/109)
- Berlind, A. A., & Weinberg, D. H. 2002, *ApJ*, 575, 587, doi: [10.1086/341469](https://doi.org/10.1086/341469)
- Bernardeau, F., Colombi, S., Gaztanaga, E., & Scoccimarro, R. 2002, *Physics Reports*, 367, 1, doi: [10.1016/S0370-1573\(02\)00135-7](https://doi.org/10.1016/S0370-1573(02)00135-7)
- Beutler, F., Saito, S., Brownstein, J. R., et al. 2014, *Monthly Notices of the Royal Astronomical Society*, 444, 3501, doi: [10.1093/mnras/stu1702](https://doi.org/10.1093/mnras/stu1702)
- Beutler, F., Seo, H.-J., Saito, S., et al. 2017, *Monthly Notices of the Royal Astronomical Society*, 466, 2242, doi: [10.1093/mnras/stw3298](https://doi.org/10.1093/mnras/stw3298)
- Bianchi, D., Burden, A., Percival, W. J., et al. 2018, *Monthly Notices of the Royal Astronomical Society*, 481, 2338, doi: [10.1093/mnras/sty2377](https://doi.org/10.1093/mnras/sty2377)
- Bose, S., Eisenstein, D. J., Hadzhiyska, B., Garrison, L. H., & Yuan, S. 2022, *Monthly Notices of the Royal Astronomical Society*, 512, 837, doi: [10.1093/mnras/stac555](https://doi.org/10.1093/mnras/stac555)
- Carlson, J., & White, M. 2010, *The Astrophysical Journal Supplement Series*, 190, 311, doi: [10.1088/0067-0049/190/2/311](https://doi.org/10.1088/0067-0049/190/2/311)
- Carrasco, J. J. M., Hertzberg, M. P., & Senatore, L. 2012, *Journal of High Energy Physics*, 2012, 82, doi: [10.1007/JHEP09\(2012\)082](https://doi.org/10.1007/JHEP09(2012)082)
- Charnock, T., Lavaux, G., & Wandelt, B. D. 2018, *arXiv:1802.03537 [astro-ph]*, <https://arxiv.org/abs/1802.03537>
- Chisari, N. E., Richardson, M. L. A., Devriendt, J., et al. 2018, *Monthly Notices of the Royal Astronomical Society*, 480, 3962, doi: [10.1093/mnras/sty2093](https://doi.org/10.1093/mnras/sty2093)
- Collaboration, D., Aghamousa, A., Aguilar, J., et al. 2016a, *arXiv:1611.00036 [astro-ph]*, <https://arxiv.org/abs/1611.00036>
- . 2016b, *arXiv:1611.00037 [astro-ph]*, <https://arxiv.org/abs/1611.00037>
- Cranmer, K., Brehmer, J., & Louppe, G. 2020, *Proceedings of the National Academy of Sciences*, 117, 30055, doi: [10.1073/pnas.1912789117](https://doi.org/10.1073/pnas.1912789117)
- Dai, B., Feng, Y., Seljak, U., & Singh, S. 2020, *Journal of Cosmology and Astroparticle Physics*, 2020, 002, doi: [10.1088/1475-7516/2020/04/002](https://doi.org/10.1088/1475-7516/2020/04/002)
- Dalal, N., Doré, O., Huterer, D., & Shirokov, A. 2008, *Physical Review D*, 77, doi: [10.1103/PhysRevD.77.123514](https://doi.org/10.1103/PhysRevD.77.123514)
- D’Amico, G., Donath, Y., Lewandowski, M., Senatore, L., & Zhang, P. 2022, *The BOSS Bispectrum Analysis at One Loop from the Effective Field Theory of Large-Scale Structure*
- Davis, M., Efstathiou, G., Frenk, C. S., & White, S. D. M. 1985, *The Astrophysical Journal*, 292, 371, doi: [10.1086/163168](https://doi.org/10.1086/163168)
- Dawson, K. S., Schlegel, D. J., Ahn, C. P., et al. 2013, *The Astronomical Journal*, 145, 10, doi: [10.1088/0004-6256/145/1/10](https://doi.org/10.1088/0004-6256/145/1/10)
- Dax, M., Green, S. R., Gair, J., et al. 2021, *Physical Review Letters*, 127, 241103, doi: [10.1103/PhysRevLett.127.241103](https://doi.org/10.1103/PhysRevLett.127.241103)
- Delgado, A. M., Wadekar, D., Hadzhiyska, B., et al. 2022, *Monthly Notices of the Royal Astronomical Society*, 515, 2733, doi: [10.1093/mnras/stac1951](https://doi.org/10.1093/mnras/stac1951)
- Desjacques, V., Jeong, D., & Schmidt, F. 2016, *arXiv:1611.09787 [astro-ph, physics:gr-qc, physics:hep-ph]*, <https://arxiv.org/abs/1611.09787>
- Eickenberg, M., Allys, E., Moradinezhad Dizgah, A., et al. 2022, *Wavelet Moments for Cosmological Parameter Estimation*
- Eisenstein, D. J., Hu, W., & Tegmark, M. 1998, *The Astrophysical Journal Letters*, 504, L57, doi: [10.1086/311582](https://doi.org/10.1086/311582)
- Eisenstein, D. J., Weinberg, D. H., Agol, E., et al. 2011, *The Astronomical Journal*, 142, 72, doi: [10.1088/0004-6256/142/3/72](https://doi.org/10.1088/0004-6256/142/3/72)
- Feldman, H. A., Kaiser, N., & Peacock, J. A. 1994, *The Astrophysical Journal*, 426, 23, doi: [10.1086/174036](https://doi.org/10.1086/174036)
- Feng, Y., Chu, M.-Y., Seljak, U., & McDonald, P. 2016, *Monthly Notices of the Royal Astronomical Society*, 463, 2273, doi: [10.1093/mnras/stw2123](https://doi.org/10.1093/mnras/stw2123)
- Font-Ribera, A., McDonald, P., Mostek, N., et al. 2014, *Journal of Cosmology and Astro-Particle Physics*, 05, 023, doi: [10.1088/1475-7516/2014/05/023](https://doi.org/10.1088/1475-7516/2014/05/023)
- Foreman, S., Coulton, W., Villaescusa-Navarro, F., & Barreira, A. 2019, *arXiv e-prints*, 1910, *arXiv:1910.03597*

- Gao, L., Springel, V., & White, S. D. M. 2005, *Monthly Notices of the Royal Astronomical Society*, 363, L66, doi: [10.1111/j.1745-3933.2005.00084.x](https://doi.org/10.1111/j.1745-3933.2005.00084.x)
- Gao, L., & White, S. D. M. 2007, *Monthly Notices of the Royal Astronomical Society*, 377, L5, doi: [10.1111/j.1745-3933.2007.00292.x](https://doi.org/10.1111/j.1745-3933.2007.00292.x)
- Garrison, L. H., Eisenstein, D. J., Ferrer, D., Maksimova, N. A., & Pinto, P. A. 2021, *Monthly Notices of the Royal Astronomical Society*, 508, 575, doi: [10.1093/mnras/stab2482](https://doi.org/10.1093/mnras/stab2482)
- Garrison, L. H., Eisenstein, D. J., Ferrer, D., et al. 2018, *The Astrophysical Journal Supplement Series*, 236, 43, doi: [10.3847/1538-4365/aabfd3](https://doi.org/10.3847/1538-4365/aabfd3)
- Germain, M., Gregor, K., Murray, I., & Larochelle, H. 2015, *Proceedings of the 32nd International Conference on Machine Learning*, 37, 881. <https://arxiv.org/abs/1502.03509>
- Green, S. R., & Gair, J. 2020, arXiv:2008.03312 [astro-ph, physics:gr-qc, stat]. <https://arxiv.org/abs/2008.03312>
- Greenberg, D. S., Nonnenmacher, M., & Macke, J. H. 2019, *Automatic Posterior Transformation for Likelihood-Free Inference*
- Grieb, J. N., Sánchez, A. G., Salazar-Albornoz, S., et al. 2017, *MNRAS*, 467, 2085, doi: [10.1093/mnras/stw3384](https://doi.org/10.1093/mnras/stw3384)
- Guo, H., Zehavi, I., & Zheng, Z. 2012, *The Astrophysical Journal*, 756, 127, doi: [10.1088/0004-637X/756/2/127](https://doi.org/10.1088/0004-637X/756/2/127)
- Guo, H., Zheng, Z., Zehavi, I., et al. 2015, *Monthly Notices of the Royal Astronomical Society*, 446, 578, doi: [10.1093/mnras/stu2120](https://doi.org/10.1093/mnras/stu2120)
- Hadzhiyska, B., Eisenstein, D., Bose, S., Garrison, L. H., & Maksimova, N. 2022, *Monthly Notices of the Royal Astronomical Society*, 509, 501, doi: [10.1093/mnras/stab2980](https://doi.org/10.1093/mnras/stab2980)
- Hadzhiyska, B., Liu, S., Somerville, R. S., et al. 2021, *Monthly Notices of the Royal Astronomical Society*, 508, 698, doi: [10.1093/mnras/stab2564](https://doi.org/10.1093/mnras/stab2564)
- Hadzhiyska, B., Eisenstein, D., Hernquist, L., et al. 2022, arXiv e-prints, arXiv:2210.10072. <https://arxiv.org/abs/2210.10072>
- Hahn, C., Beutler, F., Sinha, M., et al. 2019, *Monthly Notices of the Royal Astronomical Society*, 485, 2956, doi: [10.1093/mnras/stz558](https://doi.org/10.1093/mnras/stz558)
- Hahn, C., & Melchior, P. 2022, *Accelerated Bayesian SED Modeling Using Amortized Neural Posterior Estimation*
- Hahn, C., Scoccimarro, R., Blanton, M. R., Tinker, J. L., & Rodríguez-Torres, S. A. 2017a, *Monthly Notices of the Royal Astronomical Society*, 467, 1940, doi: [10.1093/mnras/stx185](https://doi.org/10.1093/mnras/stx185)
- Hahn, C., Vakili, M., Walsh, K., et al. 2017b, *Monthly Notices of the Royal Astronomical Society*, 469, 2791, doi: [10.1093/mnras/stx894](https://doi.org/10.1093/mnras/stx894)
- Hahn, C., & Villaescusa-Navarro, F. 2021, *Journal of Cosmology and Astroparticle Physics*, 2021, 029, doi: [10.1088/1475-7516/2021/04/029](https://doi.org/10.1088/1475-7516/2021/04/029)
- Hahn, C., Villaescusa-Navarro, F., Castorina, E., & Scoccimarro, R. 2020, *Journal of Cosmology and Astroparticle Physics*, 03, 040, doi: [10.1088/1475-7516/2020/03/040](https://doi.org/10.1088/1475-7516/2020/03/040)
- Hahn, C., Eickenberg, M., Ho, S., et al. 2022
- Hahn, C., Wilson, M. J., Ruiz-Macias, O., et al. 2022a, *DESI Bright Galaxy Survey: Final Target Selection, Design, and Validation*
- Hahn, C., Kwon, K. J., Tojeiro, R., et al. 2022b, *The DESI PRObabilistic Value-Added Bright Galaxy Survey (PROVABGS) Mock Challenge*
- Hamilton, A. J. S. 1998, 231, 185, doi: [10.1007/978-94-011-4960-0_17](https://doi.org/10.1007/978-94-011-4960-0_17)
- Hand, N., Feng, Y., Beutler, F., et al. 2018, *The Astronomical Journal*, 156, 160, doi: [10.3847/1538-3881/aadae0](https://doi.org/10.3847/1538-3881/aadae0)
- Hand, N., Li, Y., Slepian, Z., & Seljak, U. 2017, *Journal of Cosmology and Astro-Particle Physics*, 07, 002, doi: [10.1088/1475-7516/2017/07/002](https://doi.org/10.1088/1475-7516/2017/07/002)
- Harnois-Déraps, J., van Waerbeke, L., Viola, M., & Heymans, C. 2015, *Monthly Notices of the Royal Astronomical Society*, 450, 1212, doi: [10.1093/mnras/stv646](https://doi.org/10.1093/mnras/stv646)
- Hassan, S., Villaescusa-Navarro, F., Wandelt, B., et al. 2021, *HIFlow: Generating Diverse HI Maps and Inferring Cosmology While Marginalizing over Astrophysics Using Normalizing Flows*
- Hearin, A. P., Zentner, A. R., van den Bosch, F. C., Campbell, D., & Tollerud, E. 2016, *Monthly Notices of the Royal Astronomical Society*, 460, 2552, doi: [10.1093/mnras/stw840](https://doi.org/10.1093/mnras/stw840)
- Hellwing, W. A., Schaller, M., Frenk, C. S., et al. 2016, *Monthly Notices of the Royal Astronomical Society*, 461, L11, doi: [10.1093/mnrasl/slw081](https://doi.org/10.1093/mnrasl/slw081)
- Ho, S., Agarwal, N., Myers, A. D., et al. 2015, *Journal of Cosmology and Astroparticle Physics*, 2015, 040, doi: [10.1088/1475-7516/2015/05/040](https://doi.org/10.1088/1475-7516/2015/05/040)

- Hou, J., Moradinezhad Dizgah, A., Hahn, C., & Massara, E. 2022, arXiv e-prints, arXiv:2210.12743.
<https://arxiv.org/abs/2210.12743>
- Huppenkothen, D., & Bachetti, M. 2021, Accurate X-ray Timing in the Presence of Systematic Biases With Simulation-Based Inference
- Huterer, D., Kirkby, D., Bean, R., et al. 2015, *Astroparticle Physics*, 63, 23, doi: [10.1016/j.astropartphys.2014.07.004](https://doi.org/10.1016/j.astropartphys.2014.07.004)
- Ivanov, M. M., Simonović, M., & Zaldarriaga, M. 2020, *Journal of Cosmology and Astroparticle Physics*, 2020, 042, doi: [10.1088/1475-7516/2020/05/042](https://doi.org/10.1088/1475-7516/2020/05/042)
- Jain, B., Joyce, A., Thompson, R., et al. 2013, Novel Probes of Gravity and Dark Energy, arXiv, doi: [10.48550/arXiv.1309.5389](https://arxiv.org/abs/10.48550/arXiv.1309.5389)
- Jamieson, D., Li, Y., Alves de Oliveira, R., et al. 2022, Field Level Neural Network Emulator for Cosmological N-body Simulations
- Jeffrey, N., Alsing, J., & Lanusse, F. 2021, *Monthly Notices of the Royal Astronomical Society*, 501, 954, doi: [10.1093/mnras/staa3594](https://doi.org/10.1093/mnras/staa3594)
- Jespersen, C. K., Cranmer, M., Melchior, P., et al. 2022, arXiv e-prints, arXiv:2210.13473.
<https://arxiv.org/abs/2210.13473>
- Jing, Y. P., Zhang, P., Lin, W. P., Gao, L., & Springel, V. 2006, *The Astrophysical Journal Letters*, 640, L119, doi: [10.1086/503547](https://doi.org/10.1086/503547)
- Kaiser, N. 1987, *Monthly Notices of the Royal Astronomical Society*, 227, 1, doi: [10.1093/mnras/227.1.1](https://doi.org/10.1093/mnras/227.1.1)
- Kim, A., Padmanabhan, N., Aldering, G., et al. 2015, *Astroparticle Physics*, 63, 2, doi: [10.1016/j.astropartphys.2014.05.007](https://doi.org/10.1016/j.astropartphys.2014.05.007)
- Kingma, D. P., & Ba, J. 2017, arXiv:1412.6980 [cs]. <https://arxiv.org/abs/1412.6980>
- Knebe, A., Knollmann, S. R., Muldrew, S. I., et al. 2011, *Monthly Notices of the Royal Astronomical Society*, 415, 2293, doi: [10.1111/j.1365-2966.2011.18858.x](https://doi.org/10.1111/j.1365-2966.2011.18858.x)
- Kobayashi, Y., Nishimichi, T., Takada, M., & Miyatake, H. 2021, arXiv:2110.06969 [astro-ph].
<https://arxiv.org/abs/2110.06969>
- Lacerna, I., & Padilla, N. 2011, *Monthly Notices of the Royal Astronomical Society*, 412, 1283, doi: [10.1111/j.1365-2966.2010.17988.x](https://doi.org/10.1111/j.1365-2966.2010.17988.x)
- Lange, J. U., Leauthaud, A., Singh, S., et al. 2021, *Monthly Notices of the Royal Astronomical Society*, 502, 2074, doi: [10.1093/mnras/stab189](https://doi.org/10.1093/mnras/stab189)
- Laureijs, R., Amiaux, J., Arduini, S., et al. 2011, arXiv e-prints, arXiv:1110.3193
- Leauthaud, A., Bundy, K., Saito, S., et al. 2016, *Monthly Notices of the Royal Astronomical Society*, 457, 4021, doi: [10.1093/mnras/stw117](https://doi.org/10.1093/mnras/stw117)
- Lehmann, B. V., Mao, Y.-Y., Becker, M. R., Skillman, S. W., & Wechsler, R. H. 2017, *The Astrophysical Journal*, 834, 37, doi: [10.3847/1538-4357/834/1/37](https://doi.org/10.3847/1538-4357/834/1/37)
- Lemos, P., Cranmer, M., Abidi, M., et al. 2022, Robust Simulation-Based Inference in Cosmology with Bayesian Neural Networks
- Lemos, P., Jeffrey, N., Whiteway, L., et al. 2021, *Physical Review D*, 103, 023009, doi: [10.1103/PhysRevD.103.023009](https://doi.org/10.1103/PhysRevD.103.023009)
- Lesgourgues, J., Mangano, G., Miele, G., & Pastor, S. 2013, *Neutrino Cosmology*
- Liddle, A. R., & Lyth, D. H. 2000, *Cosmological Inflation and Large-Scale Structure*
- Makinen, T. L., Charnock, T., Alsing, J., & Wandelt, B. D. 2021, *Journal of Cosmology and Astroparticle Physics*, 2021, 049, doi: [10.1088/1475-7516/2021/11/049](https://doi.org/10.1088/1475-7516/2021/11/049)
- Maksimova, N. A., Garrison, L. H., Eisenstein, D. J., et al. 2021, *Monthly Notices of the Royal Astronomical Society*, 508, 4017, doi: [10.1093/mnras/stab2484](https://doi.org/10.1093/mnras/stab2484)
- Manera, M., Samushia, L., Tojeiro, R., et al. 2015, *Monthly Notices of the Royal Astronomical Society*, 447, 437, doi: [10.1093/mnras/stu2465](https://doi.org/10.1093/mnras/stu2465)
- Mao, Y.-Y., Williamson, M., & Wechsler, R. H. 2015, *The Astrophysical Journal*, 810, 21, doi: [10.1088/0004-637X/810/1/21](https://doi.org/10.1088/0004-637X/810/1/21)
- Massara, E., Villaescusa-Navarro, F., Ho, S., Dalal, N., & Spergel, D. N. 2020, arXiv:2001.11024 [astro-ph]. <https://arxiv.org/abs/2001.11024>
- Massara, E., Villaescusa-Navarro, F., Hahn, C., et al. 2022, Cosmological Information in the Marked Power Spectrum of the Galaxy Field, doi: [10.48550/arXiv.2206.01709](https://doi.org/10.48550/arXiv.2206.01709)
- Miyatake, H., More, S., Takada, M., et al. 2016, *Physical Review Letters*, 116, 041301, doi: [10.1103/PhysRevLett.116.041301](https://doi.org/10.1103/PhysRevLett.116.041301)
- Modi, C., Lanusse, F., & Seljak, U. 2021, *Astronomy and Computing*, Volume 37, article id. 100505., 37, 100505, doi: [10.1016/j.ascom.2021.100505](https://doi.org/10.1016/j.ascom.2021.100505)
- More, S., Miyatake, H., Takada, M., et al. 2016, *The Astrophysical Journal*, 825, 39, doi: [10.3847/0004-637X/825/1/39](https://doi.org/10.3847/0004-637X/825/1/39)

- Navarro, J. F., Frenk, C. S., & White, S. D. M. 1997, *The Astrophysical Journal*, 490, 493, doi: [10.1086/304888](https://doi.org/10.1086/304888)
- Papamakarios, G., Pavlakou, T., & Murray, I. 2017, arXiv e-prints, 1705, arXiv:1705.07057
- Perko, A., Senatore, L., Jennings, E., & Wechsler, R. H. 2016, *Biased Tracers in Redshift Space in the EFT of Large-Scale Structure*
- Peters, A., Brown, M. L., Kay, S. T., & Barnes, D. J. 2018, *Monthly Notices of the Royal Astronomical Society*, 474, 3173, doi: [10.1093/mnras/stx2780](https://doi.org/10.1093/mnras/stx2780)
- Philcox, O. H. E., & Ivanov, M. M. 2021, arXiv:2112.04515 [astro-ph, physics:hep-ex], <https://arxiv.org/abs/2112.04515>
- Pinol, L., Cahn, R. N., Hand, N., Seljak, U., & White, M. 2017, *Journal of Cosmology and Astroparticle Physics*, 2017, 008, doi: [10.1088/1475-7516/2017/04/008](https://doi.org/10.1088/1475-7516/2017/04/008)
- Reid, B., Ho, S., Padmanabhan, N., et al. 2016, *Monthly Notices of the Royal Astronomical Society*, 455, 1553, doi: [10.1093/mnras/stv2382](https://doi.org/10.1093/mnras/stv2382)
- Reid, B. A., Seo, H.-J., Leauthaud, A., Tinker, J. L., & White, M. 2014, *Monthly Notices of the Royal Astronomical Society*, 444, 476, doi: [10.1093/mnras/stu1391](https://doi.org/10.1093/mnras/stu1391)
- Ross, A. J., Percival, W. J., Sánchez, A. G., et al. 2012, *Monthly Notices of the Royal Astronomical Society*, 424, 564, doi: [10.1111/j.1365-2966.2012.21235.x](https://doi.org/10.1111/j.1365-2966.2012.21235.x)
- Ross, A. J., Beutler, F., Chuang, C.-H., et al. 2017, *Monthly Notices of the Royal Astronomical Society*, 464, 1168, doi: [10.1093/mnras/stw2372](https://doi.org/10.1093/mnras/stw2372)
- Rudd, D. H., Zentner, A. R., & Kravtsov, A. V. 2008, *The Astrophysical Journal*, 672, 19, doi: [10.1086/523836](https://doi.org/10.1086/523836)
- Saito, S., Leauthaud, A., Hearin, A. P., et al. 2016, *Monthly Notices of the Royal Astronomical Society*, 460, 1457, doi: [10.1093/mnras/stw1080](https://doi.org/10.1093/mnras/stw1080)
- Sargent, W. L. W., & Turner, E. L. 1977, *The Astrophysical Journal*, 212, L3, doi: [10.1086/182362](https://doi.org/10.1086/182362)
- Schaefer, D., Li, Y., Tinker, J., Ho, S., & Refregier, A. 2021, *Super-Resolving Dark Matter Halos Using Generative Deep Learning*
- Scoccimarro, R. 2000, *ApJ*, 544, 597, doi: [10.1086/317248](https://doi.org/10.1086/317248)
- Senatore, L. 2015, *Journal of Cosmology and Astroparticle Physics*, 2015, 007, doi: [10.1088/1475-7516/2015/11/007](https://doi.org/10.1088/1475-7516/2015/11/007)
- Senatore, L., & Zaldarriaga, M. 2014, *Redshift Space Distortions in the Effective Field Theory of Large Scale Structures*
- Seo, H.-J., & Eisenstein, D. J. 2003, *The Astrophysical Journal*, 598, 720, doi: [10.1086/379122](https://doi.org/10.1086/379122)
- Shao, H., Villaescusa-Navarro, F., Villanueva-Domingo, P., et al. 2022, *Robust Field-Level Inference with Dark Matter Halos*, arXiv, doi: [10.48550/arXiv.2209.06843](https://doi.org/10.48550/arXiv.2209.06843)
- Slosar, A., Hirata, C., Seljak, U., Ho, S., & Padmanabhan, N. 2008, *Journal of Cosmology and Astroparticle Physics*, 2008, 031, doi: [10.1088/1475-7516/2008/08/031](https://doi.org/10.1088/1475-7516/2008/08/031)
- Smith, A., He, J.-h., Cole, S., et al. 2019, *Monthly Notices of the Royal Astronomical Society*, doi: [10.1093/mnras/stz059](https://doi.org/10.1093/mnras/stz059)
- Somerville, R. S., & Davé, R. 2015, *Annual Review of Astronomy and Astrophysics*, 53, 51, doi: [10.1146/annurev-astro-082812-140951](https://doi.org/10.1146/annurev-astro-082812-140951)
- Spergel, D., Gehrels, N., Baltay, C., et al. 2015, *Wide-Field Infrared Survey Telescope-Astrophysics Focused Telescope Assets WFIRST-AFTA 2015 Report*
- Springel, V., Pakmor, R., Pillepich, A., et al. 2018, *Monthly Notices of the Royal Astronomical Society*, 475, 676, doi: [10.1093/mnras/stx3304](https://doi.org/10.1093/mnras/stx3304)
- Swanson, M. E. C., Tegmark, M., Hamilton, A. J. S., & Hill, J. C. 2008, *Monthly Notices of the Royal Astronomical Society*, 387, 1391, doi: [10.1111/j.1365-2966.2008.13296.x](https://doi.org/10.1111/j.1365-2966.2008.13296.x)
- Tabak, E. G., & Turner, C. V. 2013, *Communications on Pure and Applied Mathematics*, 66, 145, doi: [10.1002/cpa.21423](https://doi.org/10.1002/cpa.21423)
- Tabak, E. G., & Vanden-Eijnden, E. 2010, *Communications in Mathematical Sciences*, 8, 217, doi: [10.4310/CMS.2010.v8.n1.a11](https://doi.org/10.4310/CMS.2010.v8.n1.a11)
- Takada, M., Ellis, R. S., Chiba, M., et al. 2014, *Publications of the Astronomical Society of Japan*, 66, R1, doi: [10.1093/pasj/pst019](https://doi.org/10.1093/pasj/pst019)
- Talts, S., Betancourt, M., Simpson, D., Vehtari, A., & Gelman, A. 2020, arXiv:1804.06788 [stat], <https://arxiv.org/abs/1804.06788>
- Tamura, N., Takato, N., Shimono, A., et al. 2016, in *Ground-Based and Airborne Instrumentation for Astronomy VI*, Vol. 9908, eprint: arXiv:1608.01075, 99081M, doi: [10.1117/12.2232103](https://doi.org/10.1117/12.2232103)

- Tejero-Cantero, A., Boelts, J., Deistler, M., et al. 2020, *Journal of Open Source Software*, 5, 2505, doi: [10.21105/joss.02505](https://doi.org/10.21105/joss.02505)
- Tortorelli, L., Siudek, M., Moser, B., et al. 2021, arXiv:2106.02651 [astro-ph].
<https://arxiv.org/abs/2106.02651>
- Uria, B., Côté, M.-A., Gregor, K., Murray, I., & Larochelle, H. 2016, arXiv:1605.02226 [cs].
<https://arxiv.org/abs/1605.02226>
- Vakili, M., & Hahn, C. 2019, *The Astrophysical Journal*, 872, 115, doi: [10.3847/1538-4357/aaf1a1](https://doi.org/10.3847/1538-4357/aaf1a1)
- van Daalen, M. P., McCarthy, I. G., & Schaye, J. 2020, *Monthly Notices of the Royal Astronomical Society*, 491, 2424, doi: [10.1093/mnras/stz3199](https://doi.org/10.1093/mnras/stz3199)
- van Daalen, M. P., Schaye, J., Booth, C. M., & Dalla Vecchia, C. 2011, *Monthly Notices of the Royal Astronomical Society*, 415, 3649, doi: [10.1111/j.1365-2966.2011.18981.x](https://doi.org/10.1111/j.1365-2966.2011.18981.x)
- Villaescusa-Navarro, F., Hahn, C., Massara, E., et al. 2020, *The Astrophysical Journal Supplement Series*, 250, 2, doi: [10.3847/1538-4365/ab9d82](https://doi.org/10.3847/1538-4365/ab9d82)
- Villaescusa-Navarro, F., Ding, J., Genel, S., et al. 2022, *The Astrophysical Journal*, 929, 132, doi: [10.3847/1538-4357/ac5d3f](https://doi.org/10.3847/1538-4357/ac5d3f)
- Vogelsberger, M., Genel, S., Springel, V., et al. 2014, *Monthly Notices of the Royal Astronomical Society*, 444, 1518, doi: [10.1093/mnras/stu1536](https://doi.org/10.1093/mnras/stu1536)
- Wang, Y., Zhai, Z., Alavi, A., et al. 2022a, *The Astrophysical Journal*, 928, 1, doi: [10.3847/1538-4357/ac4973](https://doi.org/10.3847/1538-4357/ac4973)
- Wang, Y., Zhao, G.-B., Koyama, K., et al. 2022b, *Extracting High-Order Cosmological Information in Galaxy Surveys with Power Spectra*, doi: [10.48550/arXiv.2202.05248](https://doi.org/10.48550/arXiv.2202.05248)
- Wechsler, R. H., Zentner, A. R., Bullock, J. S., Kravtsov, A. V., & Allgood, B. 2006, *The Astrophysical Journal*, 652, 71, doi: [10.1086/507120](https://doi.org/10.1086/507120)
- White, M., Tinker, J. L., & McBride, C. K. 2014, *MNRAS*, 437, 2594, doi: [10.1093/mnras/stt2071](https://doi.org/10.1093/mnras/stt2071)
- White, M., Blanton, M., Bolton, A., et al. 2011, *The Astrophysical Journal*, 728, 126, doi: [10.1088/0004-637X/728/2/126](https://doi.org/10.1088/0004-637X/728/2/126)
- White, S. 2004, 30
- Wong, K. W. K., Contardo, G., & Ho, S. 2020, *Physical Review D*, 101, 123005, doi: [10.1103/PhysRevD.101.123005](https://doi.org/10.1103/PhysRevD.101.123005)
- Yuan, S., Eisenstein, D. J., & Leauthaud, A. 2020, *Monthly Notices of the Royal Astronomical Society*, 493, 5551, doi: [10.1093/mnras/staa634](https://doi.org/10.1093/mnras/staa634)
- Yuan, S., Garrison, L. H., Eisenstein, D. J., & Wechsler, R. H. 2022, *Monthly Notices of the Royal Astronomical Society*, 515, 871, doi: [10.1093/mnras/stac1830](https://doi.org/10.1093/mnras/stac1830)
- Zentner, A. R. 2007, *International Journal of Modern Physics D*, 16, 763, doi: [10.1142/S0218271807010511](https://doi.org/10.1142/S0218271807010511)
- Zentner, A. R., Hearin, A., van den Bosch, F. C., Lange, J. U., & Villarreal, A. 2016, arXiv:1606.07817 [astro-ph].
<https://arxiv.org/abs/1606.07817>
- Zhai, Z., Tinker, J. L., Hahn, C., et al. 2017, *The Astrophysical Journal*, 848, 76, doi: [10.3847/1538-4357/aa8eee](https://doi.org/10.3847/1538-4357/aa8eee)
- Zhai, Z., Tinker, J. L., Banerjee, A., et al. 2022, *The Aemulus Project V: Cosmological Constraint from Small-Scale Clustering of BOSS Galaxies*
- Zhan, H., & Knox, L. 2004, *The Astrophysical Journal Letters*, 616, L75, doi: [10.1086/426712](https://doi.org/10.1086/426712)
- Zhang, K., Bloom, J. S., Gaudi, B. S., et al. 2021, doi: [10.3847/1538-3881/abf42e](https://doi.org/10.3847/1538-3881/abf42e)
- Zheng, Z., Coil, A. L., & Zehavi, I. 2007, *The Astrophysical Journal*, 667, 760, doi: [10.1086/521074](https://doi.org/10.1086/521074)